frontiers | Frontiers in Marine Science

TYPE Original Research
PUBLISHED 11 March 2024
DOI 10.3389/fmars.2024.1308739

OPEN ACCESS

EDITED BY
Adam Thomas Devlin,
University of Hawaii at Manoa, United States

REVIEWED BY
Fajin Chen,
Guangdong Ocean University, China
Xiting Liu,
Ocean University of China, China

*CORRESPONDENCE
Zilong Li
zilongli@zju.edu.cn

RECEIVED 07 October 2023
ACCEPTED 24 January 2024
PUBLISHED 11 March 2024

CITATION
Gao Q, Piotrowski AM, Li Z, Loh PS, Han C, Wang Z, Yang S, Guo Z, Huang D and Chen Y (2024) Geochemical behavior of C, N, and S in sediments of Hangzhou Bay, Southeastern China: implications for the study of paleoclimate and sea-level changes. *Front. Mar. Sci.* 11:1308739. doi: 10.3389/fmars.2024.1308739

Geochemical behavior of C, N, and S in sediments of Hangzhou Bay, Southeastern China: implications for the study of paleoclimate and sea-level changes

Qin Gao[1], Alexander M. Piotrowski[2], Zilong Li[1]*, Pei Sun Loh[1], Cuicui Han[3], Zixuan Wang[4], Shihang Yang[5], Zengqing Guo[6], Dongqin Huang[1] and Yanting Chen[1]

[1]Institute of Marine Geology and Resources, Ocean College, Zhejiang University, Zhoushan, China, [2]Department of Earth Sciences, University of Cambridge, Cambridge, United Kingdom, [3]College of Foreign Languages, Shanghai Ocean University, Shanghai, China, [4]Tidal Flat Research Center of Jiangsu Province, Nanjing, Jiangsu, China, [5]Second Institute of Oceanography, Ministry of Natural Resources, Hangzhou, China, [6]PowerChina Huadong Engineering Corporation Limited, Hangzhou, China

The correlation between the amount of organic carbon (OC) and sulfur (S) in sediments has been widely used as a paleosalinity indicator to distinguish between marine and freshwater environments. However, whether the ratio of total OC to total S (TOC/TS) can be used to identify unsteady or dynamic marine environments across sedimentary strata is still contended. An HZW1907 sediment core of 80 m in length was successfully collected in the middle of Hangzhou Bay (HZB), serving as one of the few boreholes that are crucial for the study of geologic and geo-environment changes in the coastal regions of eastern China since the Last Glacial Maximum (LGM). Total OC (TOC), stable carbon isotope, and TS of 82 subsamples from the HZW1907 core were analyzed to reconstruct the history of the shallow water biological pump and sulfur preservation record in the bay since the Late Pleistocene. Our results indicate that the samples had low concentrations of TOC (0.21%) and total nitrogen (TN) (0.02%), high mass ratio of TOC/TN (10.8), low $\delta^{13}C$ (–24.9‰), low TS content (0.06%), and a high ratio of TOC/TS (9.1) from 33.6 ka BP to 12.3 ka BP, implying that freshwater organic matter (OM), algae, and C3 plant fragments were the main sources of OM in a relatively cold environment. The abundances of TOC, TN, and TS increased to 0.56%, 0.07%, and 0.4%, respectively, while $\delta^{13}C$ (–23.9‰) increased and TOC/TS (2.7) decreased in the Holocene sediments, suggesting that seawater began to influence the composition of the sediments of HZB. Climate warming, which is likely to have impacted the results, was experienced from 12.3 ka BP. An OC isotope mixing model indicated that since the Mid-late Holocene, more than 70% of riverine OM accounted for the total OM. The TOC/TS ratio was identified as an effective indicator of seawater intrusion, with C/S ratios of 1–6 being considered to indicate a "sea–land transitional zone" sedimentary environment, a C/S >6 indicating freshwater,

and a C/S<1 indicating normal marine facies. These findings provide crucial evidence for using TOC/TS to distinguish freshwater from marine environments and enhance our understanding of past climate changes. Therefore, these geochemical indicators can be used in conjunction with other sedimentary records to obtain accurate results about sedimentary evolution.

KEYWORDS

organic carbon, sulfur biogeochemistry, sea level, delta-shelf-estuary system, climate change, Hangzhou Bay

1 Introduction

The continental margin is the active terrestrial–ocean interface that serves as a primary location for the biochemical and sedimentary cycling of organic carbon (OC), nitrogen (N), and sulfur (S) (Berner, 1982; Jørgensen and Kasten, 2006; Hu et al., 2011; DeLaune and White, 2012; Hu et al., 2014; Jørgensen et al., 2019; Chen et al., 2021). Dynamic physicochemical reactions along continental margins create complex OC–N–S cycles that can be affected by local climate; however, the mechanistic link of climate change to the OC–N–S cycles is not well understood (Mcleod et al., 2011; Liu Q. et al., 2018; Liu X. T., et al., 2018; Sun et al., 2020; Liu X. T., et al., 2021; Wang et al., 2021; Zhao et al., 2021; Liu et al., 2023). The sedimentary process on the continental margin is primarily controlled by the change in sea level, with different sedimentary sequences forming at different sea levels. Therefore, sedimentary deposition on the continental margin is very sensitive to sea-level fluctuations, making it one of the most widely analyzed factors in the reconstruction of ancient sea-level conditions. In the absence of micropaleontological fossils and sedimentary structures, authigenic minerals and geochemistry may provide useful insights. Previous studies have shown that the content of pyrite sulfur and the ratio of total sulfur to total organic carbon (TS/TOC, hereby written as C/S) can indicate sea-level changes (Hepp et al., 2019; Liu et al., 2020; Liu X. T., et al., 2021; Liu X. T., et al., 2021; Obrist-Farner et al., 2021; Chang et al., 2023). Typical marine sediments are characterized by an average C/S of 2.8 ± 1.5 (Berner, 1984; Raiswell and Canfield, 2012), and this ratio has been successfully applied to tracing environmental evolution of continental shelves and estuaries since the last deglaciation (Liu X. T., et al., 2018; Liu et al., 2022). However, the C/S ratios of the shallow nearshore sediments are much higher than 2.8 along the inner shelf of the East China Sea (ECS), which has been attributed to the unsteady diagenetic processes where strong physical reworking leads to abnormally low sulfide production, such as that found in freshwater environments (Lambeck et al., 2014; Ge et al., 2015; Zhu et al., 2016). Therefore, we need to evaluate the applicability of the C/S ratio as an indicator of marine transgression under the influence of unsteady diagenetic processes on a longer time scale, particularly in dynamic marine environments (Li et al., 2013; Fike et al., 2015).

The Eastern China Marginal Seas (ECMS) are typical shelf marginal seas that are characterized by complicated sedimentation and hydrodynamic processes (refer to Figure 1A). In addition to terrestrial inputs, multiple currents driven by the East Asian monsoon and tides occur in the ECMS and interact in a dynamic manner (Li et al., 2004; Zhang et al., 2009). Recent studies measured the C–N–S chemistry of organic matter (OM) in the ocean surface and core sediments of the ECMS (Liu and Zheng, 2017; Yuan et al., 2017; Loh et al., 2018; Liu et al., 2020; Chang et al., 2023; Jiang et al., 2023; Wang et al., 2023). These studies investigated OM sources, paleoclimate conditions, sedimentary dynamics, oceanic circulation patterns, and paleoproductivity such as C and S preserved in ECMS sediments. They also examined C/S and C/N ratios together, revealing the depositional evolution in terrestrial and marine environments, which are sensitive to sea-level and climatic changes (Liu Y. et al., 2021).

Hangzhou Bay (HZB) is connected to the Qiantang River (QTR), the Yangtze River Delta (YRD), and the East China Sea Shelf (ECSS). HZB is a dynamic and complex source-to-sink system in strong tidal environments (Zhang et al., 2014; Liu Y, et al., 2021), which makes it a suitable area for studying Late Quaternary sedimentary processes. Some studies have examined HZB, focusing on the characteristics of sediment fillings and the evolution of sedimentary facies, provenance systems, geomorphic formations, and shallow gas (Lin, 1997; Lin et al., 2004; Liu et al., 2006; Liu et al., 2017; Lin and Zhang, 2018; Chen et al., 2020; Liu Y., 2021; Zhang et al., 2021). Most of these studies aimed to quantitatively reveal and predict correlations among erosion, transportation, and final deposition of sediment in response to perturbations caused by climate, sea-level fluctuations, and other forcing parameters on different temporal and spatial scales. The accumulation of fine-grained sediments in such a tidal-dominated area also creates a unique geological pool for sedimentary C–N–S matter that has not been adequately studied systematically (Liu X. T., et al., 2021; Jiang et al., 2023). In this study, we present new C–N–S data from the HZW1907 core obtained from HZB with the objective of improving our understanding of C–N–S variance with sea-level and paleoclimate changes in the East China Sea. This study also aims to identify the implication of variance in C–N–S for the evolution of the tidal-dominated depositional environment since the last deglaciation.

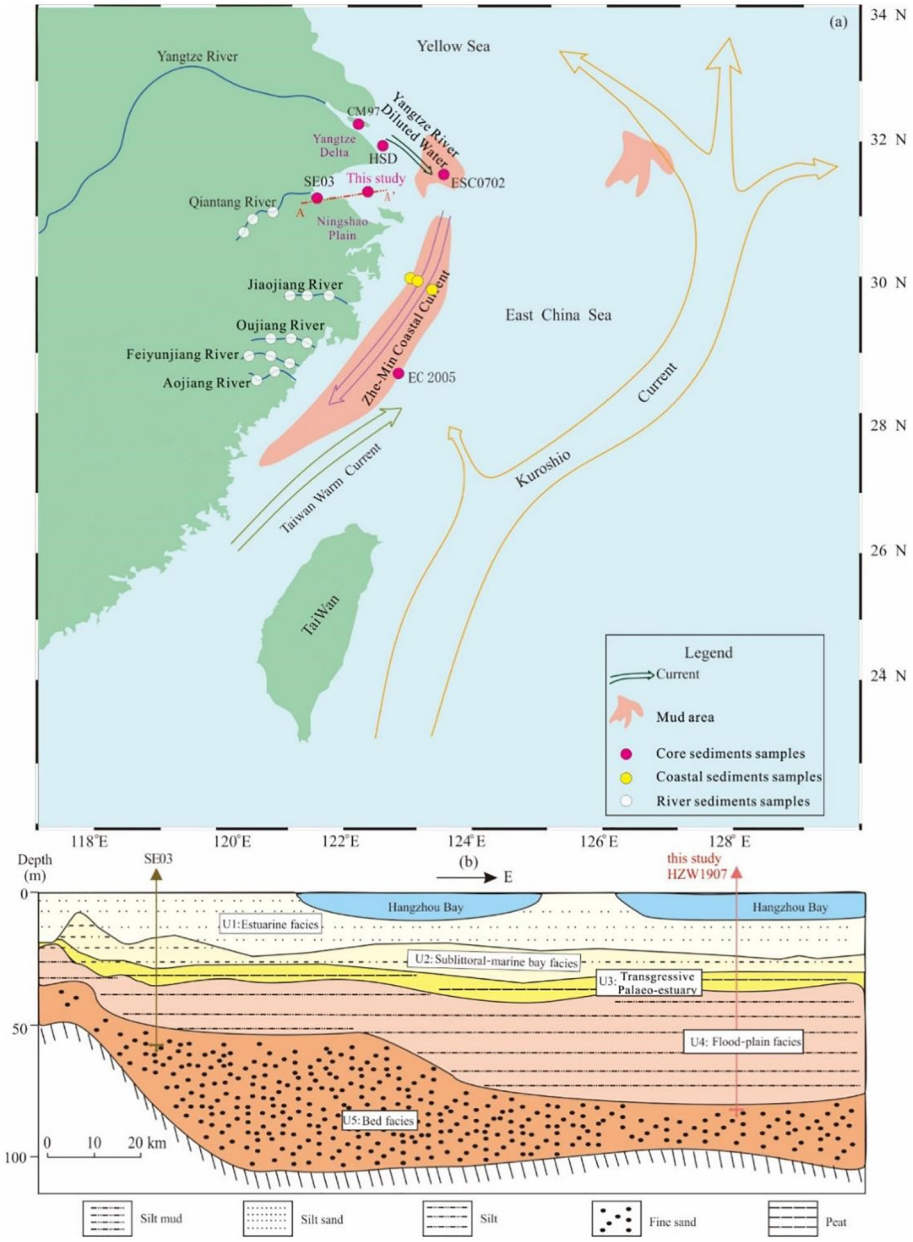

FIGURE 1
(A) Locations of the sediment cores in this study, adapted from Liu X. T. et al. (2021). Current system and mud area in the East China Sea and rivers flowing into the sea, adapted from Bi et al. (2015). **(B)** Cross-section A–A′ of the late Quaternary Qiantang incised valley fill, adapted from Lin et al. (2004) and Zhang et al. (2015). The SE03 core in the inner of HZB (Jiang et al., 2023), CM97 (Tang et al., 2006) and HSD cores in YRD (Chen et al., 2021), EC2005 core in ECSS, and river and coastal sediments in Zhejiang Province (Liu X. T., et al., 2021).

2 Geological and regional background

Geologically, the QTR drainage and HZB are situated in the northeast part of the South China Plate. They are divided by the Jiangshan–Shaoxing fault into two main tectonic domains: the northwestern part, which forms the Qiantang depression within the Yangtze Block, and the southeastern part, which forms the Cathaysia fold belt in the Cathaysia Block (Shu et al., 2015).

HZB is a trumpet-shaped estuary formed by the QTR entering the East China Sea. It faces the southern part of the YRD in the north and the Ningshao Plain in the south (see Figure 1A). The width of HZB varies considerably, ranging from ~100 km to ~20 km (Xu, 1995). The emergence of HZB is directly related to sea-level changes that have occurred since the Late Pleistocene (Chen et al., 1990). During the Last Glacial Maximum (LGM: 26.5~19.0 ka BP), the sea level was ~130 m below the present-day sea level, and the area was incised to form a 60–100-m valley (Lin et al., 2004). The stratigraphic architecture of HZB fills has been studied in detail (Lin et al., 2004; Zhang et al., 2014; Lin and Zhang, 2018; Gao et al., 2023). From the bottom to the top, the sedimentary succession of the valley can be divided into five sedimentary units (refer to Figure 1B). These are the amalgamated fluvial channel (U5), the

floodplain and channel complex (U4) that accumulated before ca. 13.0 cal kyr BP, a transgressive paleoestuary (U3; ca. 13.0–8.0 cal kyr BP), an offshore shallow-marine phase (U2) that formed during the time of maximum transgression (8.0–6.0 cal kyr BP), and the modern highstand estuary (U1; 6.0 cal kyr BP to present) (Gao et al., 2023). The U5 section consists mainly of sandy gravels that have the coarsest mean grain size and few plant fragments. The gravels vary in composition: they include quartzite, tuff, sandstone, chert, and acid volcanic rocks. The sediments in U4 alternate between (sandy) mud and fine sand with peat layers and abundant plant fragments. The U3 sediments are primarily composed of grayish-yellow or gray mud and sandy mud. Wavy, lenticular, and horizontal beddings are common. Foraminiferal fossils are present and are mainly composed of agglutinated benthic foraminifera (BF) including *Textularia* spp. and *Reophax* spp. Some euryhaline (BF) with vitreous shells such as *Ammonia beccarii* appear locally. Unit U2 mainly consists of soft mud containing abundant shallow-marine benthic foraminifera (e.g., *Elphidium magellanicum* and *Cribrononion vetreum*) and circular to elliptical burrow. U1 is mainly composed of fine sand and sandy mud, with the color changing from gray at the bottom to yellowish gray at the top. Wavy bedding is common, and plant fragments are scattered throughout the muddy sediments. Foraminiferal fossils dominated by BF are also abundant in these facies. More than 30 BF species are identified, including *Ammonia beccarii* vars., *Elphidium advenum*, *Ammonia compressiuscula*, *Ammonia koeboeen sis*, and *Ammonia ketienziensis*. They are primarily euryhaline, with vitreous shells (Zhang et al., 2014; Gao et al., 2023).

The present-day deposition system in HZB comprises a confluence of sediment from the QTR and the YRD, and marine sedimentary material causes high deposition rates (Zhang et al., 2014; Zhang et al., 2015; Liu X. T., et al., 2021). Most of the particulate matter is trapped in the inner HZB, transported by the Qiantang River. However, there are larger amounts of fine-grained materials that are deposited in the outer HZB, where YRD particulate matter is transported and deposited through the coagulation of clays, tidal action, and interaction with the southward-flowing Zhe-Min coastal current (Lian et al., 2016; Zhang et al., 2019). Following the post-glacial rise in sea level, HZB developed into an estuary (Lin, 1997; Shu et al., 2010; Lin et al., 2015; Zhang et al., 2015; Lin et al., 2022). The seaward extension of the coastline on the southern arm of the YRD has allowed the outer HZB to transform from a shallow marine environment to an open bay environment (Chen et al., 1990). The HZW1907 core analyzed in this study was obtained from the transfer area on the outer maritime space of HZB (see Figure 1A).

3 Materials and methods

The HZW1907 core (30°24′16′′N, 121°29′50′′E, water depth of ca. 10 m) was obtained in July 2019 by drilling a borehole at the outer HZB (location is shown in Figure 1). The total length of the core was 84.0 m (refer to Figure 2). Previous studies had systematically determined particle size, foraminifera, ^{14}C dating, and the geochemical characteristics of organic and inorganic elements along the sediment core (Huang et al., 2022; Gao et al., 2023).

To determine the TOC, TN, and stable carbon isotope, approximately 50 mg of the ground samples were measured into 1.5 ml micro test tubes. Sediments were digested using 1 M of HCl to remove inorganic carbon from the sediments. This was achieved using a pipette to add an adequate amount of HCl into the micro test tubes, and the mixture was stirred carefully to ensure the acid was thoroughly mixed with the sediments. The samples were left overnight to ensure that the reaction went to completion. Samples were allowed to settle to ensure that the acid separated from the residue, facilitating the removal of the HCl. A pipette was used to extract the acid, and then the residue was flushed with distilled water, stirred, allowed to settle, and removed from the solution. The rinsing process was repeated three times until the pH was neutral or approaching neutral. After this, the samples were placed in an oven and dried at 45°C for 2 days. The dried product was ground using an agate mortar and pestle. After rehomogenization, 20 mg (± 5 mg) was weighed into 12 × 4 × 4 mm aluminum weighing boats that were folded using precleaned forceps (contact-free to ensure no cross-contamination) and crushed under a stainless steel weight. These were placed in a sample tray and sent for bulk elemental and carbon isotope analysis. TOC and TN were then normalized to weight in grams as a fraction of sample weight and then standardized as percentages for conversion to TOC% and TN%. The $\delta^{13}C$ data were reported using the conventional delta notation in per mil (‰) as per the Vienna Pee Dee Belemnite (VPDB) standard. Before analysis, the bulk sediments were dried and ground into powder. Approximately 0.5 g of powder for each sample was dissolved in 10% hydrochloric acid to remove the inorganic carbon (carbonate). The carbonate-free samples were then analyzed to determine the percentage weight of TOC and TN. The samples were determined by an EA-IsoLink elemental analyzer with a MAS 200R autosampler coupled to a MAT253 plus isotope ratio mass spectrometer via a ConFlo IV universal interface (all from Thermo Fisher Scientific Branch, Bremen, Germany).

For TS measurement, 0.5 g of dry sediment sample was weighed into micro test tubes. In the presence of flux of high-purity iron powder and air ventilation at 1,250°C–1,300°C, high-temperature cauterization decomposition occurred, generating SO_2, which was absorbed by water to form sulfurous acid. We utilized starch as an indicator and conducted a titration using an iodine standard titration solution to determine the amount of sulfur in the sample using an elemental analyzer (Multi EA 4000, Germany). The detection limit of the tested standard solution was 0.04 mg/kg, and the relative deviations of the contents of 0.5 mg/kg and 1.5 mg/kg in the laboratory were 3%–5%.

4 Results

Detailed stratigraphy, sedimentology, clay mineralogy, and paleoenvironmental analyses of the HZW1907 core have been reported (Huang et al., 2022; Gao et al., 2023). Based on the age model, the sedimentation rates at the top section of the HZW1907 core (0–84 m) vary between 0.10 m/ky and 7.78 m/ky, with an

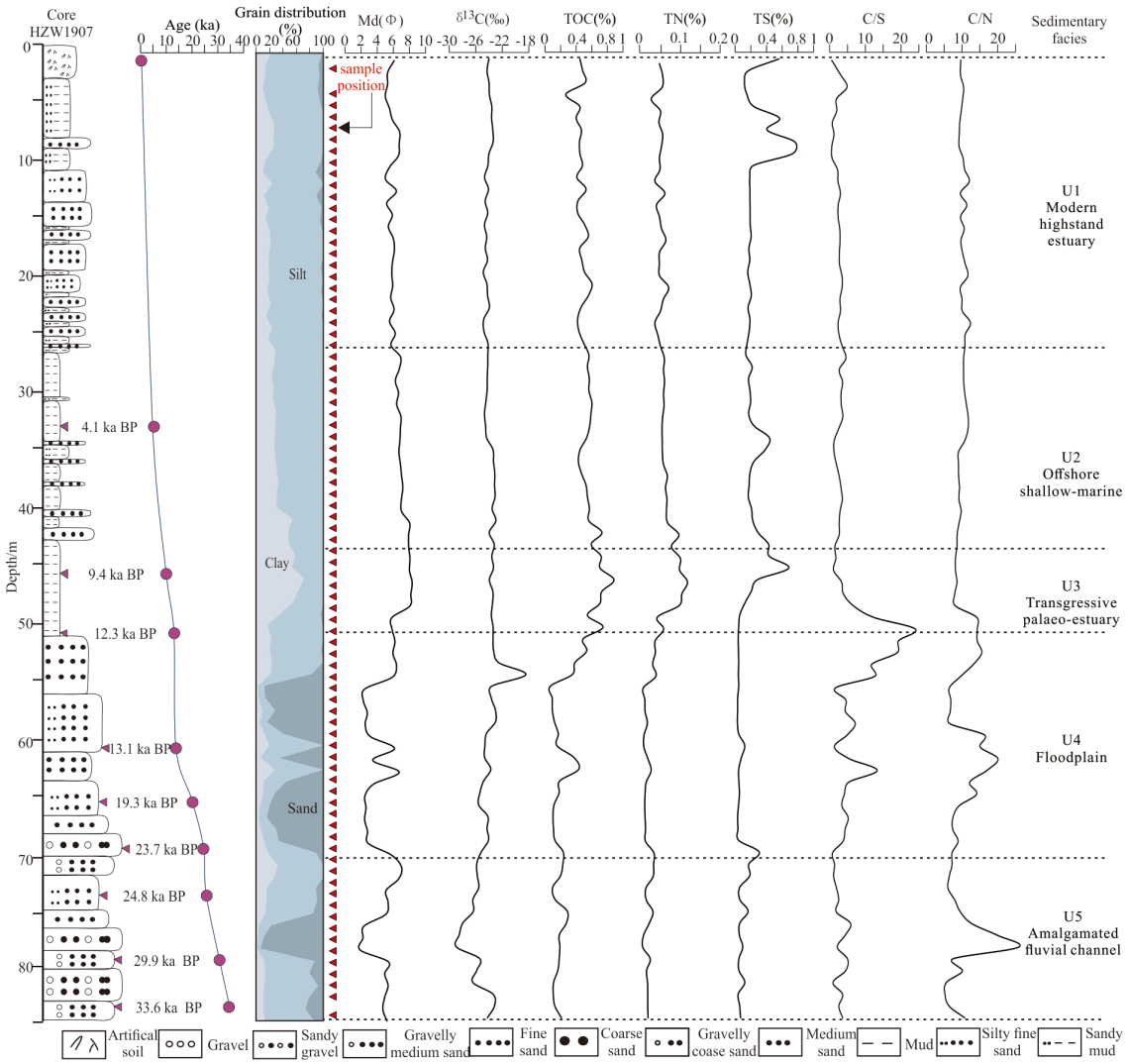

FIGURE 2
Downcore variations in $\delta^{13}C$, total organic carbon (TOC) content, total nitrogen (TN) content, total sulfur (TS) content, C/S ratio, and C/N ratio of the HZW1907 core. Note: Lithology, ^{14}C age, grain composition, and sedimentary facies for core HZW1907, adapted from Gao et al. (2023).

average of 2.46 m/ky having been deposited since 33.6 ka BP (see Figure 2). The results reveal that the sedimentary environment of the core, especially since 33.6 ka, was continuous for terrigenous sediment input. The mean grain size (Mz) of the HZW1907 core varies between 1.9 Φ and 8.3 Φ, and it exhibits irregular downcore variations. The bottom fluvial facies consist of the coarsest sand with minor gravels, with an Mz of 4.8 Φ. The Mz gradually fluctuates more from the fluvial facies up to the floodplain facies that comprise sediments of approximately 2.5 Φ~7.0 Φ. The transgressive paleoestuary facies consist of the finest sediments of approximately 8.0 Φ. The Md in offshore shallow marine facies is coarser than U3 with 6.7 Φ. However, the modern highstand facies at the top become coarser, with an average Mz of approximately 5.8 Φ (refer to Figure 2; Gao et al., 2023).

Detailed results of the $\delta^{13}C_{OC}$, TOC, TS, C/S ratio, and C/N ratio along the depth of the HZW1907 core are provided in the Appendix (Supplementary Table S1) and shown in Figure 2. Organic carbon $\delta^{13}C$ values in the HZW1907 core ranged from −29.1‰ to −18.5‰. It is divided into three groups (see Figure 2): i) The first group was deposited in the Late Pleistocene (33.6~12.3 ka BP), exhibiting relatively large fluctuations with a range of −18.51‰ to −28.09‰ in the U4 and U5 sediments. ii) The second group was deposited between 12.3 ka BP to 9.0 ka BP, consisting of the U3 stage, exhibiting a constant $\delta^{13}C$ value (−24.03‰ to −23.04‰). iii) The third group exhibited a $\delta^{13}C$ value that fluctuated between −24.90‰ and −23.10‰ in the U2 and U1 sediments. The lower mean $\delta^{13}C$ value was −24.9‰ in the U5 and U4 sediments during the Last Glacial Maximum (LGM: 26.5~19.0 ka BP), but increased to −24.00‰ in U3, U2, and U1 sediments during the Holocene.

The TOC content is less than 0.22% in U5, with a mean value of 0.16%. The TOC content in U4 ranges between 0.05% and 0.74% (with an average of 0.25%), which was slightly higher than in U5. The TOC content of U3 is the highest in the middle of the core, ranging from 0.56% to 0.89% (with an average of 0.70%). In U2 and U1, the TOC content decreases to ranges of 0.42% to 0.60% (with an average of 0.53%) and 0.39% to 0.60% (with an average of 0.46%), respectively.

The TS varies from the bottom to the top of the borehole. The TS content of U1 to U3 is distinctly higher than that at the bottom in U4 and U5 (see Figure 2). At the bottom in the U4 and U5 stages, the TS content is mostly no higher than 0.1%, with average values of 0.03% and 0.09%, respectively. The TS content in U2 ranges from 0.16% to 0.43%, with an average value of 0.21%. The average TS content in the U1 stage is 0.26%, ranging from 0.11% to 0.76%.

The mean C/S ratio exhibits a continuous decline from 9.87 to 2.34 in the five sediment units (see Table 1; Figure 2). A rapid decrease in the mean C/S ratio (from 9.87 to 2.87) is observed in the Late Pleistocene and early Holocene (33.6~9.0 ka BP). Then, the mean C/S ratio exhibits a slight decrease from 2.87 to 2.34. The C/N ratio varies between 8.37 and 11.75 and can be divided into two units (see Figure 2; Table 1): the lower sections (U5 to U4), which are characterized by dramatic fluctuations from 5.15 to 25.97, and the upper sections (U3 to U1), which exhibit smooth changes (7.92 to 12.37), separated by a transition section (U3).

5 Discussion

5.1 Sensitivity of organic matter to environmental changes

TOC/TN and $\delta^{13}C$ serve as effective indicators of environmental evolution (Zong, 2004; Milne et al., 2009; Milliman and Farnsworth, 2011; Blair and Aller, 2012; Chang et al., 2023). Researchers posit that climate affects the preservation and transportation of OM. However, these paleoenvironmental proxies are currently predominantly employed in studies involving lacustrine and deep-sea sediments, as well as loess, where depositional environments are relatively straightforward, and the sedimentary stratigraphy is relatively continuous. The applicability of TOC/TN and $\delta^{13}C$ in investigations of deltaic areas, characterized by more complex sedimentary environments, warrants careful consideration. The sediments in HZB are crucial for examining the sensitivity of OM proxies, owing to the unique tidal environment in the area.

From the bottom to the top, the strata of the HZW1907 core consist of bedding facies (U5, approximately 33.6 ka BP and 23.9 ka BP), floodplain facies (U4, approximately 23.9 to 12.3 ka BP), paleoestuary facies (U3, approximately 12.3 to 9.5 ka BP), shallow-sea facies (U2, approximately 9.5 to 6.0 ka BP), and modern estuary facies (U1, approximately 6.0 ka BP to present). These five units can be categorized into two stages: one is a freshwater deposition stage from U5 to U4, and the other is a seawater deposition stage from U3 to U1. The freshwater deposition stage exhibits a TOC and TN content range similar to the Yangtze River estuary (shown in Figure 3A), suggesting the input of terrigenous OM sources during the lower sea levels of the Late Pleistocene in the East China area. In contrast, during the seawater deposition stage, a comparable range of TOC and TN content is observed in the inner shelf of the East China Sea (see Figure 3A), indicating that the material originated from marine-derived OM due to the rising sea levels since the Holocene. From the freshwater deposition stage to the seawater deposition stage, the TOC and TN contents show an increase, but the ratio of C/N decreases (refer to Figure 3A). This trend aligns with the geochemistry observed in sediments from the contemporary Yangtze River estuary–East China Sea Shelf system (C/N = 4.98~13.44, Tesi et al., 2007; Hu et al., 2009; Hu et al., 2012). Consequently, the recorded variations in TOC and TN within U3 to U1 samples can be interpreted as indicative of marine-derived OM in U3 to U1 samples. Considering the distinct climatic region and the drainage basin characteristic of other large rivers worldwide (see Figure 3A), the observed declining TOC/TN ratio in this core since 33.6 ka BP may be attributed to biological productivity, potentially linked to climate variations. However, it is crucial to note that further evidence is needed to substantiate this interpretation.

The relationship between the organic $\delta^{13}C$ and the molar TOC/TN ratio is indicative of the different OM sources that contributed to deposits in the HZW1907 core, suggesting changes experienced in the sedimentary environment since the Late Pleistocene (see Figure 3B). The TOC/TN ratio varies between 5.15 and 25.98 and the mean value of $\delta^{13}C$ is less than −26‰ in U5, indicating that terrestrial OM mixed with freshwater OM, algae, and soil OM from the QTR catchment in 33.6 to 23.7 ka BP (refer to Figure 3B). The TOC/TN ratio varies between 6.36 and 21.15 and the mean value of $\delta^{13}C$ is −23.77 in U4. Therefore, C3 vascular plant detritus is higher than in U5, and plant detritus was observed in U4 (Gao et al., 2023). The plant detritus appears in U4 (23.9 to 12.3 ka BP), suggesting that the sediment environment changed from a river channel into a floodplain (Li et al., 2008; Wang et al., 2019; Lin et al., 2022). The range of $\delta^{13}C$ values and TOC/TN in U3–U1 is indicative of contributions of a mixture of terrestrial and marine OM sources, with the former being predominant (see Figure 3B). This finding indicates that there was a more substantial deposition of terrestrial OM in HZB that can be attributed to the significant contribution of suspended matter from the Yangtze River (Zhang et al., 2021). This significant mixing effect of marine and riverine OM was also

TABLE 1 Average values of carbon, nitrogen, and sulfur of the HZW1907 core sediments from HZB.

Sediment unit	$\delta^{13}C$ (‰)	TOC (%)	TN (%)	TS (%)	TOC/TS	TOC/TN
U1 (approximately 6.0 ka BP to present)	−24.27	0.46	0.05	0.26	2.34	10.26
U2 (approximately 9.5 to 6.0 ka BP)	−24.00	0.53	0.06	0.21	2.87	10.23
U3 (approximately 12.3 to 9.5 ka BP)	−23.56	0.70	0.10	0.32	2.87	8.37
U4 (23.9 to 12.3 ka BP)	−23.77	0.26	0.02	0.03	8.34	11.75
U5 (33.6 and 23.9 ka BP)	−26.03	0.17	0.02	0.09	9.87	9.87

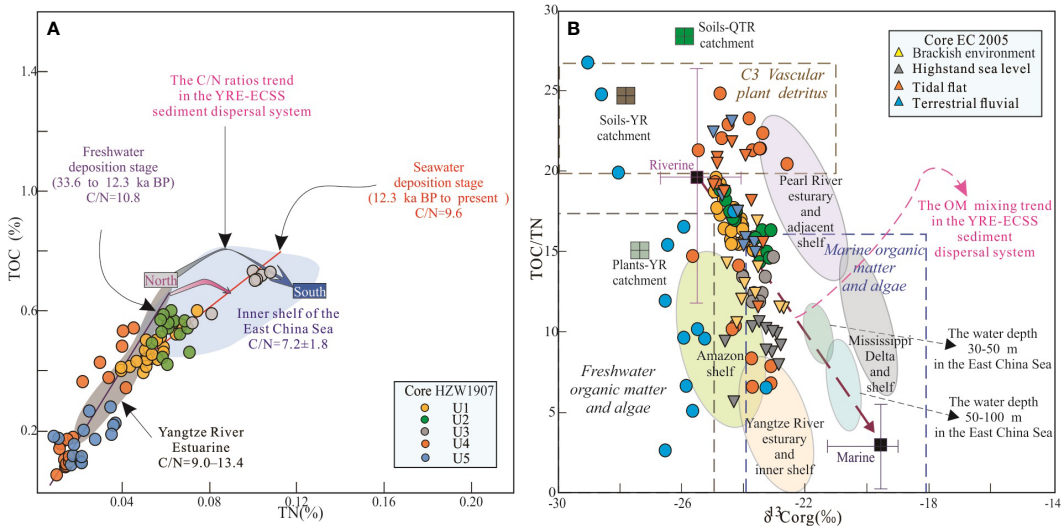

FIGURE 3
(A) The scatter plot of TOC and TN in the HZW1907 core sediment samples, compared with modern sediments in ECSS, adapted from Wu et al. (2007). **(B)** The range in weight C/N and $\delta^{13}C$ values for the main sources of organic matter in HZW1907 at different stages, adapted from Lamb et al. (2006). Data of the Yangtze River estuary and inner shelf from Liu et al. (2020); soils-YR catchment, plants-YR catchment from Wu et al. (2007); riverine from Liu et al. (2007); soils-QTR catchment from Liu et al. (2017); marine from Liu X.T. et al. 2018; OM in different water depths from Wang et al. (2021); Amazon shelf (Showers and Angle, 1986); Mississippi Delta and adjacent shelf (Bianchi et al., 2002); and Pearl River estuary (Hu et al., 2006).

observed at the Yangtze River estuary and its adjacent shelf as well as the Pearl River estuary and its adjacent shelf (see Figure 3B; Li et al., 2012; Wang et al., 2021; Sun et al., 2022). However, the terrigenous OM in HZB is deeper than that of the Pearl River estuary, as measured using organic carbon isotope analysis (shown in Figure 3B). When the results are compared to those regarding the contemporary sedimentary OM at different water depths in ECSS, a linear relationship for the mixture of marine and riverine OM is obtained, which aligns with the terrestrial–marine OM mixing hypothesis (Hedges and Oades, 1997; Goñi et al., 1998; Perdue and Koprivnjak, 2007).

Therefore, a two-end-member mixed model with organic carbon isotope is employed to calculate the relative proportion of terrestrial and marine OM sources (Equations 1, 2). Appropriate maritime end-member $\delta^{13}C$ values were selected to assess the contribution from U3 to U1 during the seawater depositional stage. One end member comprises suspended particle OM from the deep chlorophyll maximum layer of the inner shelf of the southern ECS (Liu Q. et al., 2018; Liu X. T., et al., 2018). The other consists of the OM found in the form of particulate matter in the Yangtze River (Liu et al., 2020), which is believed to have a significant influence on the YRD, the HZB, and the ECSS since the Holocene (Bi et al., 2015; Zhang et al., 2021; Gao et al., 2023). The following equations summarize the contributions of these two end members:

$$\delta^{13}C_{org} = C_R * \delta^{13}C_{org}R + C_M * \delta^{13}C_{org}M \quad (1)$$

$$C_R + C_M = 1 \quad (2)$$

where C_R and C_M denote the proportion of riverine and marine OM, respectively, and $\delta^{13}C_{org}R$ and $\delta^{13}C_{org}M$ represent their $\delta^{13}C$ value end members (see Table 2). Riverine and marine end members are −25.6 and −20.6, respectively.

The results from the mixing model indicate a predominant increase in riverine-derived OM from the sediments of U3 to U1. The riverine-derived OM remains distinct in these three deposition units, with the fractions of riverine OM in U1 and U2 being 68% and 74%, respectively (Table 2), both exceeding that in U3 (59%).

The sediments in U3 (12.3 ka BP to 9.0 ka BP) are interpreted as being deposited in a paleoestuarine or tidal flat sedimentary environment. The higher percentage of marine-derived OM in U3 may have resulted from favorable environments for the production or preservation of marine OM (Hedges and Oades, 1997) and weak riverine transport due to strong East Asian winter monsoons triggered by a YD cooling event (Liu et al., 2017). This suggests that paleoclimate variations possibly influenced the changes during the fast transgression period in the Asian margin region.

During the U2 stage (9.0 ka BP to 6.0 ka BP), over 30% of marine-derived OM was deposited and preserved due to the presence of fine-grained sediment with high sedimentation rates (see Figure 2; Burdige, 2007). These high percentages of marine-derived OM suggest a depositional environment characterized by continuous seawater filling (Hori et al., 2001; Dong et al., 2020).

The contribution of riverine OM contribution is from 68% in U2 to 78% in U1. This upward trend in riverine OM can be associated with the strengthening of the river's carrying capacity, particularly the southward transport of materials by the Yangtze since the mid-late Holocene (Zhang et al., 2015; Zhang et al., 2019; Wang et al., 2023). In addition, East Asia monsoon events may have also played a role in the accumulation of riverine organic carbon in the estuary area (Cao et al., 2018; Zhao et al., 2019; Jiang et al., 2023).

10.3389/fmars.2024.1308739

TABLE 2 The Holocene OM contribution from riverine and marine OM contributions in the ECSS sedimentary system.

Sediments Units and end member	TOC/TN molar ratio Range (mean)	$\delta^{13}C$ (‰) Range (mean)	Marine OM contribution Range (mean %)	Riverine OM contribution Range (mean %)	References
The outer of HZB (this study)					
U1	9.1~12.4 (10.3)	−24.9~ −23.5 (−24.3)	14~42 (26)	58~86 (74)	This study
U2	9.0~11.7 (10.2)	−24.8~ −23.2 (−24.0)	16~48 (32)	52~84 (68)	
U3	7.9~9.1 (8.4)	−24.0~ −23.0 (−23.6)	32~52 (41)	48~68 (59)	
The inner of HZB (core SE03)					
Paleoestuary		−25.2~24.6 (−24.9)	9~20 (14)	80~91 (86)	Jiang et al. (2023)
Storm deposit		−25.6~ −25.3 (−25.3)	1~8 (5)	92~99 (95)	
Shallow marine		−23.3~ −25.2 (−24.0)	7~47 (31)	53~93 (69)	
East China Sea Shelf (core EC2005)					
Brackish environments	7.0~10.2 (7.8)	−24.6~ −22.8 (−23.5)	21~53 (42)	47~79 (58)	Liu et al. (2020)
Highstand sea level	6.6 to 8.9 (7.3)	−24.6~ −22.8 (−23.5)	22~43 (43)	43~78 (57)	
Tidal flat	7.5 to 15.5 (9.8)	−25.0~ −22.7 (−23.8)	19 ~ 59(36)	41 ~ 81(64)	
Yangtze River Delta (core CM97)					
Delta	6.7~9.8 (8.3)	−24.9~ −24.1 (−24.5)	13~31 (22)	69~87 (78)	Tang et al. (2006)
Shallow marine	5.3~6.2 (5.8)	−24.6~ −24.1 (−24.2)	20~33 (27)	67~80 (78)	
Paleoestuarine	4.5~7.3 (5.9)	−24.5~ −24.1 (−24.3)	22~32 (27)	68~78 (78)	
QTJ	7.9~10.5 (9.2)	−27.0			Loh et al. (2018); Liu et al. (2017)
Yangtze River estuary	6.3~11.1 (9.8)	−27.0	14	86	Zhao et al. (2021); Sun et al. (2022)
Water depth 30–50 m in ECS			72	28	Wang et al. (2021)
Water depth 50–100 m in ECS			86	14	
Riverine end members	8.3~25.0 (12.5)	−26.3~ −24.9 (−25.6)	0~8 (4)	100~92 (96)	Wu et al. (2007)
Marine end members	5.3~6.3 (5.5)	−21.8~ −19.4 (−20.6)	100	0	Liu Q. et al. (2018); Liu X. T., et al., 2018

Similarly, the mixing model results show a pattern of changes in the mixture of terrestrial and marine OM with variations in Holocene sea levels in the river–coastal–shelf sediments system (refer to Figure 4). This suggests depositional environments characterized by gradual landward inundation by seawater.

HZB (41% for the HZW1907 core) and the ECSS (36% for the EC2005 core) exhibit greater marine OM contributions than the QTR estuary (14% for the SE03 core) and the YRD (27% for the CM97 core) during 13~8 ka BP. The signal for marine organic carbon was observed at 13.1 ka BP in the ECSS (the EC2005 core) sediments (Liu et al., 2020), while the outer HZB (the HZW1907 core) and the Yangtze Estuary (the HSD core) sediments were influenced by marine organic carbon in approximately 12.5~12.3 ka BP. The sea level increased from −60 to −50 in 600–800 years, at an average rising rate of 16.6 mm/a to 12.5 mm/a. This result is similar to the 15-mm/a change observed in the ECSS for the same period

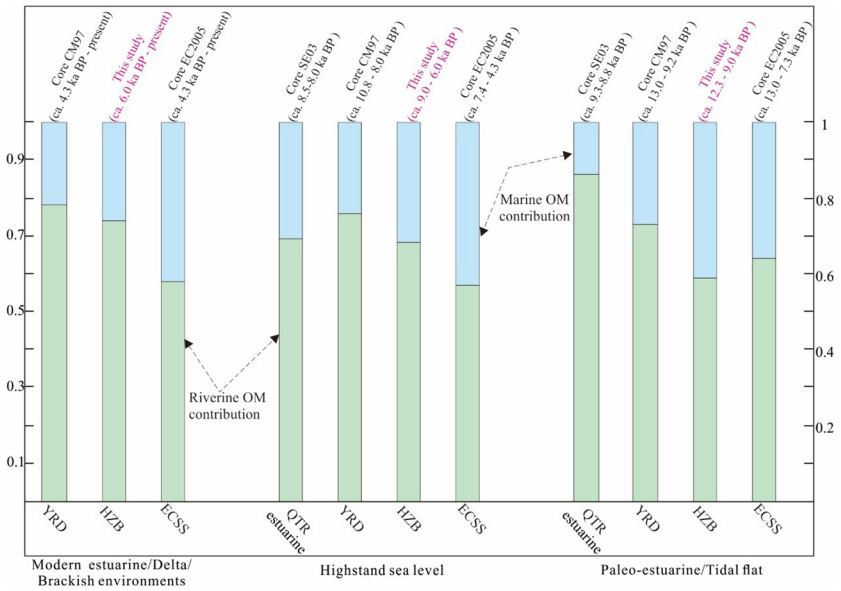

FIGURE 4
The $\delta^{13}C$ mixing model results for Holocene riverine and marine OM contributions in the East China River–coastal shelf sedimentary systems. Typical core locations are seen in Figure 1. The SE03 core in the inner of HZB (Jiang et al., 2023), the CM97 core in YRD (Tang et al., 2006), and the EC2005 core in ECSS (Liu X.T. et al. 2021).

(Mix et al., 2001; Li et al., 2014; Li et al., 2017). Therefore, in the ECSS, the transition from terrestrial to marine facies is effectively identified using organic matter. In 8~4 ka BP, all core sediments experienced a notable increase in marine OM contributions compared with the sediments in 13~8 ka BP, suggesting homogeneous sea–land interactive sedimentary environments. The YRD (CM97) exhibited the lowest marine contribution due to the substantial transport of land-based material from the Yangtze River during this period (Hori et al., 2001; Li et al., 2014; Cao et al., 2018). In the late Holocene (4 ka BP to present), there was a gradual decrease in marine OM contributions from the YRD (0.22 for the CM97 core), HZW (0.26 for the HZW1907 core), and the ECSS (0.42 for the EC2005 core), indicating that interactive sedimentary environments formed from 4 ka BP in the East China coast. This sedimentary mode in the ECSS is similar to that in the contemporary southward dispersal system by the Yangtze River and East China Sea (Hu et al., 2012).

Overall, the increasing TOC and TN composition, decreasing gradient of the C/N ratios, and $\delta^{13}C$ are crucial records that can enhance our understanding of seawater intrusion in the sediments of the East China coast. The organic matter in core sediments exhibits useful sensitivity to deep-time environmental evolution in the Yangtze River estuary–Hangzhou Bay–inner shelf dispersal systems.

5.2 The evolution of sulfur: its use as a paleosalinity archive

Paleosalinity reconstructions are important in paleoenvironment, paleoclimate, and paleoecological studies (Ingram et al., 1996; Raiswell and Canfield, 2012; Algeo et al., 2015; Wei and Algeo, 2020; Ouyang et al., 2023). The salinity of water bodies in estuarine coastal zones is subject to the effects of terrestrial river flushing and seawater (Dávila et al., 2002); consequently, sediment paleosalinity reconstruction in such areas is more difficult than in stable marine or lacustrine areas. The fluid salinity difference between the QTR estuary and the adjacent shallow sea is nearly 280 times (Lin and Zhang, 2018; Xu et al., 2019). Reconstructing the evolution of salinity since the Late Pleistocene deposition processes is crucial for enhancing our understanding of the sedimentary environment; the cycling of elements such as carbon, nitrogen, and sulfur; and sea-level changes in the land–sea interaction zone.

The sulfate ion content in freshwater is generally low, at a mean value of approximately 0.027 mmol/L (Berner, 1984). In comparison, sulfate (SO_4^{2-}) is the main form of sulfur in seawater, at an average amount of up to 29 mmol/L (Algeo et al., 2015; Gomes and Johnston, 2017). Seawater sulfate is the world's largest sulfur reservoir, and it enters marine sediments driven by organic matter mineralization in the marginal sea (Jørgensen et al., 2019). The relationship between sulfur and carbon in sediments can reflect changes in the sedimentary environment, with the changes primarily relating to the salinity of the water (Kitamura et al., 2019). The use of the relationship between sulfur and carbon as an indicator relies on the assumption that sulfide, which is produced by organoclastic sulfate reduction (OSR; Equation 3), is limited by organic carbon instead of sulfate and iron (Morse and Berner, 1995).

$$SO_4^{2-} + 2CH_2O \rightarrow H_2S + 2HCO_3^- \quad (3)$$

However, low C/S ratios or a poor correlation between these two elements, which are usually considered indicators of euxinic conditions (Raiswell and Canfield, 2012), could also be caused by

the enrichment of sulfur due to the anaerobic oxidation of methane (AOM; Equation 4).

$$CH_4 + SO_4^{2-} \rightarrow HCO_3 - + HS^- + H_2O \quad (4)$$

Both $\delta^{13}C$ (‰) and C/N values indicate the entry of marine OM into HZB from the U3 stage, transforming the sediment into a crucial "sink" for seawater OM. A recent examination of the modern depositional system suggests that, for sediments containing >0.5% organic carbon, C/S ratios reaching a value of 10 can effectively distinguish freshwater deposits from brackish and marine deposits (Wei and Algeo, 2020). When plotting the combined TOC and TS content for the HZB and adjunction marine sediments, no obvious correlation between TOC and TS content is observed (refer to Figure 5), suggesting that pyrite sulfur is not sorely derived from sulfate reduction driven by the oxidation of organic carbon (Equation (3), OSR). This suggests that pyrite sulfur may come from a sulfate-driven AOM process (Equation 4).

Sediments from the QTJ estuary, outer HZB, and ECSS mud belt undergo distinct C and S preserving processes. Unit 5 and unit 4 in the HZW1907 core (approximately 33.6~12.3 ka BP) exhibit a high ratio of C/S (more than 8) and are positioned below the regression line of C/S ratio = 2.8 ± 1.5 (see Figure 5D). This suggests that core sediments from units 5 and 4 were deposited in a freshwater environment. When juxtaposed with C/S results from the SE03 and EC2005 cores, these findings suggest that the depositional systems of the Qiantang River estuary–Hangzhou Bay–East China Sea Shelf were predominantly influenced by freshwater transport and depositional processes prior to the Holocene.

The East China Sea Shelf and the Eastern China estuarine area underwent gradual inundation by seawater from the Holocene (Li et al., 2014). The C/S ratio in U3 declined rapidly, possibly triggered by a shallow suboxic–anoxic boundary resulting from a high sedimentation rate, attributed to brackish water intrusion (Boetius et al., 2000; Zheng et al., 2011; Sato et al., 2012). During the period (12.3~9.0 ka BP), the C/S ratio in the QTR estuary (the SE03 core) and the ECSS (the EC2005 core) decreased synchronously. However, both the QTR estuary and HZB experienced more intense fluctuations, exhibiting lower C/S ratios than the ESCC (refer to Figure 5C), suggesting that the higher sedimentation rate induced sulfate reduction by facilitating an OSR process (Chen et al., 2020; Liu et al., 2020; Yang et al., 2022). The significant fluctuation in C/S indicates that particle size plays a crucial role in OM preservation (Bianchi et al., 2018). Lin et al. (2004) suggested

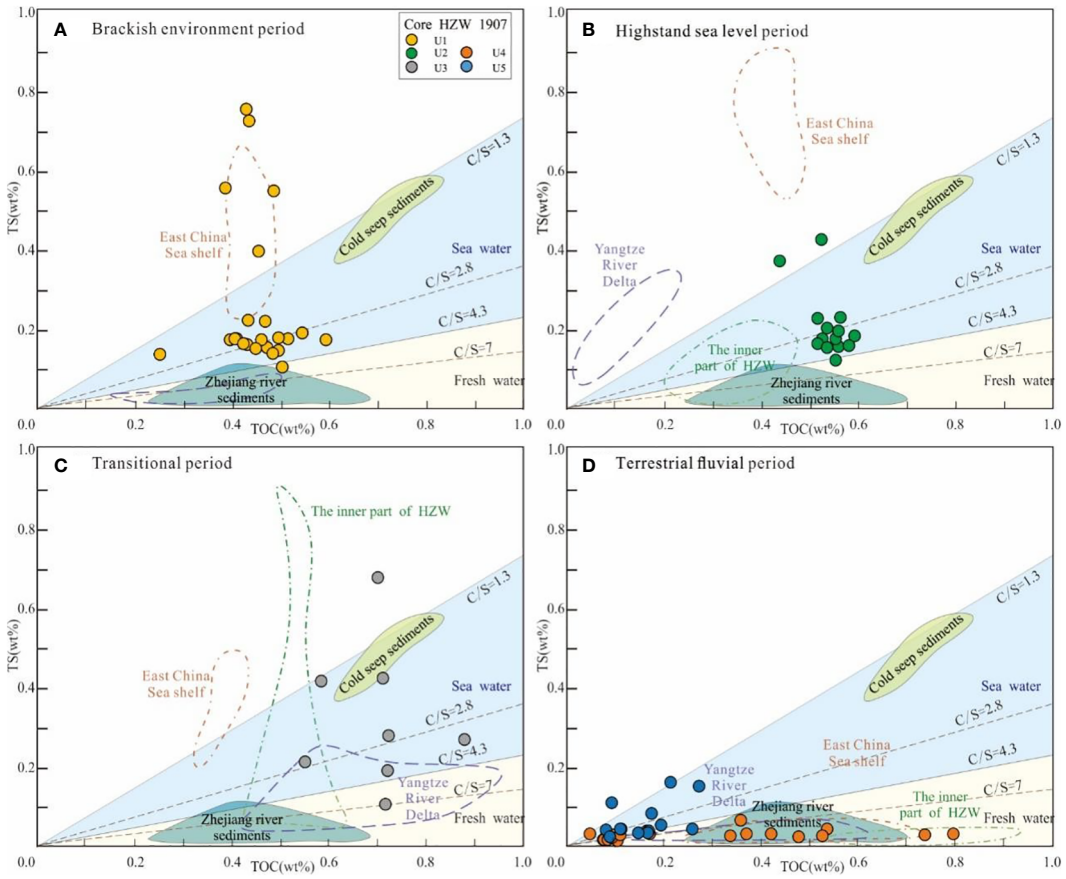

FIGURE 5
Scatter plot of TOC versus TS content for different sedimentary stages, adapted from Liu X. T. et al. (2021). **(A)** Brackish environment period; **(B)** High sea level period; **(C)** Transitional period; **(D)** Terrestrial period. The C/S ratio of 2.8 ± 1.5 represents modern normal marine sediments (Berner, 1984), while the C/S ratio of 7 indicates mobile tropical deltaic muds (Aller, 2014). The core SE03 core in the inner of HZW (Jiang et al., 2023), core CM97 (Tang et al., 2006), core HSD in YRD (Chen et al., 2021), and core EC2005 in ECSS (Liu X. T. et al., 2021) are shown in Figure 1. The TOC and TS contents of coastal sediment samples (Ge et al., 2015) and cold seep sediments (Sato et al., 2012) are presented for comparison.

that the floodplain facies (U4) is a promising target for shallow biogenic gas and continuing emission into U3 in the HZB area; therefore, the AOM process would also promote sulfur preservation in U3.

Almost all sediments from unit 2 (ca. 9.0~6.0 ka BP) are situated above the regression line of C/S ratio = 2.8 ± 1.5, and the majority fall within the normal range of marine deposition (refer to Figure 5B). The stable C/S ratio ranging from 2.8 to 4.3 in U2 is interpreted as indicating a highstand sea level, suggesting a sustained seawater condition (Arndt et al., 2013). Compared with the early Holocene (12.3~9.0 ka BP), a noticeable increase in deposited sulfur is observed through the declining C/S ratio in U2, implying a gradual strengthening of the OSR and AOM processes (e.g., pyrite; Leavitt et al., 2013).

In the mid-late Holocene (approximately 6.0 ka BP), most sediments from unit 1 are situated above the regression line of C/S ratio = 2.8 ± 1.5 (see Figure 5A), suggesting a normal marine deposition environment. The notably low C/S ratios (<0.5) in U1 may be attributed to more extensive AOM processes compared with U2, stemming from the eruption of methane originating from U2 and U4 (Lin et al., 2015; Song et al., 2023).

Aqueous Sr, which is present in much higher concentrations in seawater than in freshwater, is readily adsorbed onto clay minerals and, to a lesser degree, organic matter and Fe-ox hydroxides, resulting in substantially higher Sr/Ba ratios in marine sediments compared with freshwater sediments (Shen et al., 2015). The amounts of Sr and Ba in the HZW1907 core were published by Gao et al. (2023), who indicated that the ratio of Sr/Ba in U5 and U4 is lower than 0.2, while C/S values are relatively high, suggesting that freshwater depositional environments are involved in the U5 and U4 stages (refer to Figure 6). The ratio of Sr/Ba in U1 and U2 was higher than 0.25, while C/S values were lower, suggesting seawater depositional environments in the U1 and U2 stages. The ratio of Sr/Ba in the U3 stage was between 0.2 and 0.25, indicating a transitional environment from freshwater to seawater. In summary, despite being affected by various diagenetic processes, freshwater and marine environments dominate the differential TS contents (see Figures 5, 6). We strongly advocate the systematic use of C/S proxies to support paleosalinity interpretations.

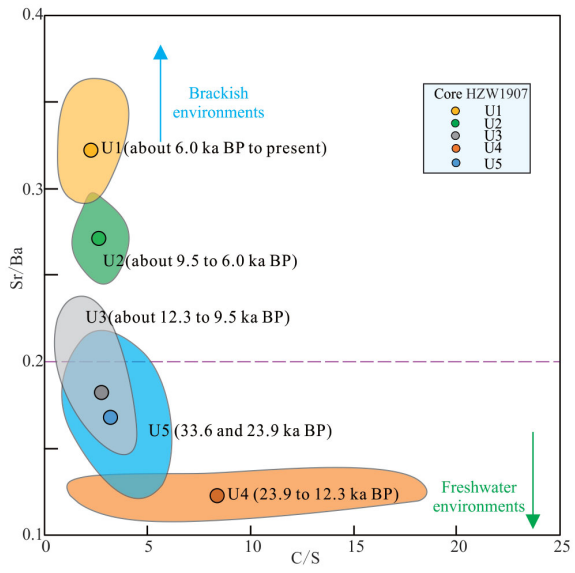

FIGURE 6
Discrimination plot of C/S versus Sr/Ba for the bulk sediments of the HZW1907 core. Element contents of Sr and Ba for the sediments from Gao et al. (2023). The purple dotted line is the boundary between freshwater and brackish environments, where Sr/Ba is 0.2 according to Wei and Algeo (2020).

5.3 C–N–S in HZB: implications for the study of the East China River–coastal shelf sedimentary systems

As an important conjunction with the ECSS, HZB contains crucial evidence that can inform discussions on how depositional evolution impacts the preservation of nitrogen, carbon, and sulfur, as well as the variation of the three elements with climate and sea-level changes. The elements Cr and Th are reliable indicators in the reconstruction of the East China River–coastal shelf sedimentary systems, its sediment source-to-sink transport processes, and major controlling mechanisms involved since the Pleistocene. The inner shelf mud and HZB sediments predominantly originated from the Changjiang River when there were lower sea levels in the Holocene, and were significantly affected by the Zhe–Min Rivers when there were high sea levels in the late Pleistocene (Bi et al., 2017; Zhang et al., 2021; Gao et al., 2023). The sediments of the U5 and U4 stages in the HZW1907 core are more felsic, and they have lower Cr/Th levels, indicating that sediments were deposited from the Qiantang River basin when the area had lower sea levels (Gao et al., 2023). In periods when the sea level was higher, the sediments of U3 to U1 are more mafic, suggesting that Changjiang mud either reached the Qiantang River valley directly by southward advection of the freshwater plume of the Changjiang or was resuspended from the inner-shelf mud wedge and transported landward into the Qiantang River system by flood tidal currents and sea waves (Zhang et al., 2021). The composition of sedimentary organic matter ($\delta^{13}C$, TOC/TN, TOC/TS) also provides evidence for the marine transgression of coastal areas (see Figures 7A–C). However, the mass ratio of total organic carbon and total sulfur (C/S ratio, R^2 = 0.8) is a more sensitive proxy for seawater intrusion than organic carbon isotope (R^2 = 0.1), total organic carbon, and total nitrogen (R^2 = 0.6). Similarly, interpretations obtained by examining TOC concentration, TOC/TN, and TOC/TS in the HZW1907 core are consistent with those obtained from interpretations of the ratio of Mg/Ti, which has been used to examine paleoclimate changes (see Figures 7D-F; Nesbitt and Young, 1982; Roy and Roser, 2013; Zhang et al., 2013; Gao et al., 2023). The changes in Mg/Ti objectively reflect climatic variations in the source area, which is affected by the evolution of the East Asian monsoon (refer to Figure 6; Wang et al., 2001; Rasmussen et al., 2014; Tao et al., 2016; Cheng et al., 2020; Zhou et al., 2022). The stalagmite oxygen isotope records from approximately 34.0 ka BP indicate that the summer monsoon became increasingly warmer despite the appearance of several cooling events (Wang et al., 2005). As the climate warmed, the Mg was steadily enriched but Ti in the

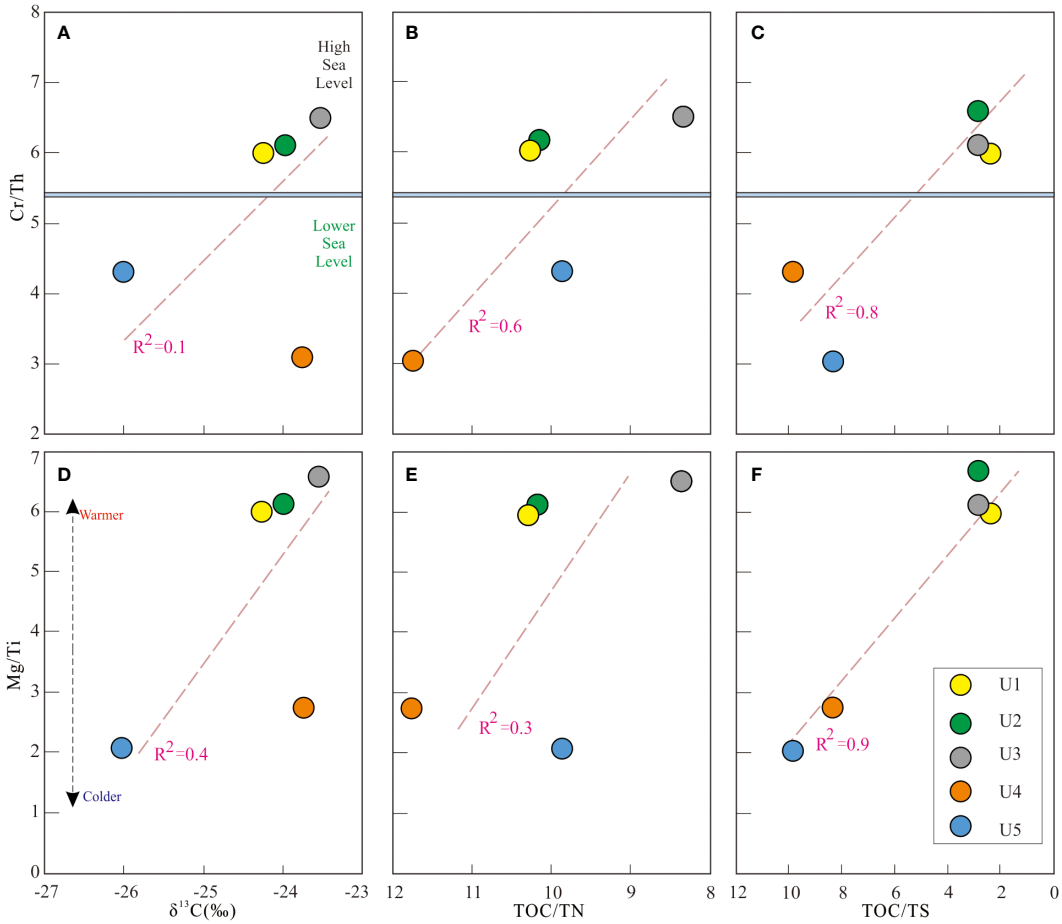

FIGURE 7
Correlations of organic matter with indices of sea-level change and weathering indices in HZB sediments **(A–F)**. The relationship indicates the sea-level change by climate warming control on organic matter characteristics. Element contents of Cr, Th, Mg, and Ti for the sediments in core HZW1907 from Gao et al. (2023).

weathering products. The $\delta^{13}C$, TOC/TN, and TOC/TS in the core sediments exhibit some positive correlation with Mg/Ti, suggesting that the strengthening monsoon climate was a crucial factor that had a significant influence on the inputs of OM in the estuary. This sensitivity of organic matter fractions to monsoon climate had also been observed in the deposition in the Pearl River estuary (Zong et al., 2006). The weak variation of sedimentary organic matter in the Changjiang Estuary to the Holocene monsoon variability may be caused by large water and sediment fluxes, rapid accumulation, and increasing anthropogenic activities since 14 ka BP (Zhou et al., 2006). However, the correlation between climate and organic matter deposition was found to be strong in the HZW1907 core, where freshwater constantly mixed with brackish-salt water since the Holocene. Therefore, the depositional setting in the estuary and inner shelf may be a sink that can provide crucial information on climactic changes, particularly regarding the deposition of particulate organic matter.

Previous studies have demonstrated that C/S and C/N ratios, which are sensitive to sea-level and climatic changes in the ECS inner shelf (Liu X. T., et al., 2021; Chang et al., 2023), can be examined together to reveal the depositional evolution from terrestrial to marine environments. Additionally, as mentioned above, the content of OM in the HZW1907 core is likely to be limited by the condition of the environment. There are relatively apparent correlations between C/S and C/N ratios in sediments and the ratio of Cr/Th, with their R^2 being more than 0.6 (see Figures 7B, C). Additionally, there is a robust correlation between C/S and C/N ratios and Mg/Ti (R^2 = 0.9 and 0.3, respectively; refer to Figures 7E, F) for climate change, suggesting that the C/S ratio can be used more sensitively to distinguish between freshwater and marine/brackish environments.

The C/N and C/S ratios indicate that the sediments in units 5 and 4 of the HZW1907 core were deposited in a terrestrial freshwater environment. OM deposited in this period comprises freshwater organic matter, algae, and C3 vascular plant detritus (see Figure 3B), representing a typical terrestrial fluvial/lacustrine environment. Terrestrial components dominate in the region, which is indicated by the elevated C/N ratios (Hu et al., 2007; Acharya et al., 2015; Chen et al., 2015). The strong oxidation conditions also generate particularly low TS content in the freshwater environment. Consequently, almost all values of C/S ratio are higher than 6 (refer to Figure 8), corresponding to the

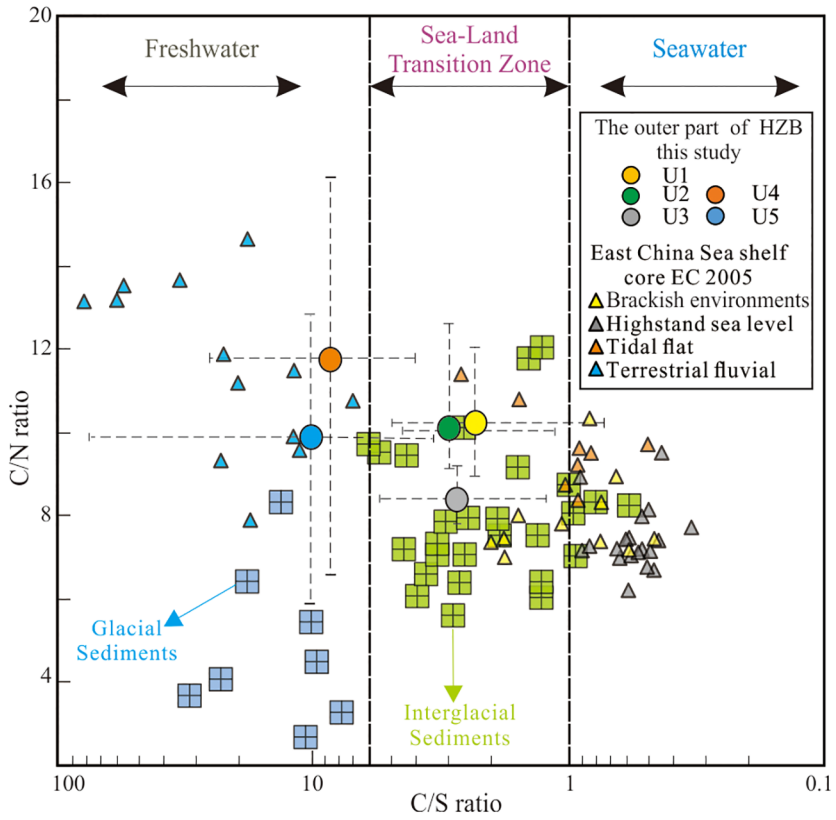

FIGURE 8
The mean values of C/S and C/N ratios and the range of the HZW1907 core indicate environmental evolution. The core EC2005 from Liu X. T. et al. (2021); Zhejiang coast (Sanmen Bay) glacial and interglacial sediments in the NDGK2 core from Chang et al. (2023).

recently proposed S/TOC threshold of 0.1 (Wei and Algeo, 2020), as well as results from the terrestrial fluvial sediments (17.3–13.1 ka BP) in the EC2005 core (Liu et al., 2022) and the Zhejiang coast (Sanmen Bay) glacial sediments (Chang et al., 2023). Both C/S and C/N ratios in unit 3 declined from 7 to 1.3, indicating a transitional environment from a terrestrial to a marine environment in the early Holocene, during which seawater intensified OSR and AOM processes (Berner, 1984; Boetius et al., 2000). This result was observed in the EC2005 core from the ECSS (see Figure 8; Liu X. T. et al., 2021). Units 2 and 1 were deposited in a normal marine environment, which is significantly different from that found in the ECSS (the EC2005 core; Liu X. T. et al., 2021), but is relatively similar to interglacial sediments in the NDGK2 core obtained from the Zhejiang coast (Chang et al., 2023). These results suggest that HZB sediments were deposited in a "sea–land transitional zone" rather than in a brackish environment such as that in the ECSS (refer to Figure 7) even though organic carbon isotope signatures revealed more sea-sourced OM substances in U2.

In summary, the depositional conditions of the study area were impacted by sea-level changes that could significantly influence the C–N–S conditions. The C/N and C/S ratios can provide supplementary evidence for identifying the sedimentary environment for the East China River–coastal shelf sedimentary systems. A C/S ratio of less than 1 is relatively normal in a seawater environment, while that greater than 8 is normal in a freshwater environment. In comparison, a "sea–land transitional zone" sedimentary environment often has a C/S ratio ranging from 1 to 6 (shown in Figure 8). However, there is a need for further investigations on the chemical and isotopic composition of pore water obtained from different geological and marine backgrounds.

6 Conclusion

Due to the transition of their sedimentary environment from a terrestrial to a marine environment since the last deglaciation, the HZB and its adjacent sea areas provide an ideal natural laboratory for the study of the link among carbon, nitrogen, and sulfur with significant alongshore sediment dispersal. Alongside the results from samples of the ECSS core sediments and river sediments, our results reveal that C–N–S levels in the HZW1907 core sediments vary due to marine transgression and that the sedimentation process could significantly impact the diagenetic path.

1) The mass ratios of TOC, TN, and $\delta^{13}C$ in the HZW1907 core suggest a river-dominated organic carbon deposition process. The TOC/TN ratio and $\delta^{13}C$ content are shown to be sensitive to sea levels in the Yangtze River estuary–Hangzhou Bay inner shelf dispersal systems. The TOC and TN content in the HZW1907 core exhibits an increasing gradient pattern accompanied by a decreasing gradient for C/N ratios, suggesting large inputs of

organic matter, with the supply of the organic matter since the Last Glacial Period being from different sources. Freshwater organic matter, algae, and C3 plant fragments are the main sources of organic matter in U5 and U4 (33.4–12.3 ka BP). The impact of marine organic matter or marine algae is evident in their absorption into U3–U1 since 12.3 ka BP. The $\delta^{13}C$ mixture model for the HZW1907 core indicates that riverine OM in U1 and U2 are 68% and 74%, respectively, with the proportions of both in U1 and U2 being greater than they are in U3 (59%). Additionally, the $\delta^{13}C$ mixture model is a relatively effective factor for identifying organic matter sources in the Yangtze River estuary–HZB inner shelf dispersal systems.

2) The gradient of C/N and C/S ratios can serve as supplementary indicators for identifying the characteristics of sedimentary environments, including identifying freshwater and brackish environments present since the Late Pleistocene along the East China Sea coast. However, the C/S ratio is a more effective indicator of seawater intrusion. We propose a C/S ratio of less than 1 to 2.8 to be considered a normal seawater environment, while that greater than 8 can be considered a normal freshwater environment. Additionally, for the Yangtze River estuary–HZB inner shelf dispersal systems, we propose that a C/S ratio between 1 and 6 can be considered a "sea–land transitional zone" sedimentary environment. The results of this study indicate that identifying marine transgressions and their magnitude using C–N–S amounts has significant value in deep-time studies of the paleoenvironment, even though the results require verification through further study.

Data availability statement

The datasets presented in this study can be found in online repositories. The names of the repository/repositories and accession number(s) can be found in the article/Supplementary Material.

Author contributions

QG: Writing – original draft, Conceptualization, Data curation, Investigation, Methodology, Validation. AP: Writing – review & editing, Conceptualization, Supervision, Validation. ZL: Writing – review & editing, Conceptualization, Data curation, Funding acquisition, Investigation, Methodology. PL: Writing – review & editing. ZW: Writing – review & editing, Data curation. CH: Writing – review & editing. SY: Methodology, Writing – review & editing. ZG: Investigation, Writing – review & editing. DH: Data curation, Methodology, Writing – review & editing. YC: Data curation, Methodology, Writing – review & editing.

Funding

The author(s) declare financial support was received for the research, authorship, and/or publication of this article. This work was supported by the Zhejiang University Education Foundation Global Partnership Fund (Grant No. 100000-11320).

Acknowledgments

The authors express their appreciation to PowerChina Huadong Engineering Corporation Limited, for facilitating the collection of HZW1907 core sediments, and extend thanks to Dr. Sangana Peter for his valuable assistance.

Conflict of interest

Author ZG is employed by the company PowerChina Huadong Engineering Corporation Limited, Hangzhou.

The remaining authors declare that the research was conducted in the absence of any commercial or financial relationships that could be construed as a potential conflict of interest.

Publisher's note

Supplementary material

The Supplementary Material for this article can be found online at: https://www.frontiersin.org/articles/10.3389/fmars.2024.1308739/full#supplementary-material

References

Acharya, S. S., Panigrahi, M. K., Gupta, A. K., and Tripathy, S. (2015). Response of trace metal redox proxies in continental shelf environment: The Eastern Arabian Sea scenario. *Continent. Shelf Res.* 106, 70–84. doi: 10.1016/j.csr.2015.07.008

Algeo, T. J., Luo, G. M., Song, H. Y., Lyons, T. W., and Canfield, D. E. (2015). Reconstruction of secular variation in seawater sulfate concentrations. *Biogeosciences* 12 (7), 2131–2151. doi: 10.5194/bg-12-2131-2015

Aller, R. (2014). "Sedimentary Diagenesis, Depositional Environments, and Benthic Fluxes," in *Treatise on Geochemistry*, *2nd ed.* Eds. H. Holland and K. K. Turekian (Oxford: Elsevier), 293–334.

Arndt, S., Jørgensen, B. B., LaRowe, D. E., Middelburg, J., Pancost, R., and Regnier, P. (2013). Quantifying the degradation of organic matter in marine sediments: a review and synthesis. *Earth-Sci. Rev.* 123, 53–86. doi: 10.1016/j.earscirev.2013.02.008

Berner, R. A. (1982). Burial of organic carbon and pyrite sulfur in the modern ocean; itsgeochemical and environmental significance. *Am. J. Sci.* 282, 451–473. doi: 10.2475/ajs.282.4.451

Berner, R. A. (1984). Sedimentary pyrite formation: an update. *Geochem. Cosmochim. Acta* 48, 605–615. doi: 10.1016/0016-7037(84)90089-9

Bi, L., Yang, S. Y., Li, C., Guo, Y. L., Wang, Q., Liu, J. T., et al. (2015). Geochemistry of river-borne clays entering the East China Sea indicates two contrasting types of weathering and sediment transport processes. *Geochem. Geophys. Geosys.* 16, 3034–3052. doi: 10.1002/2015GC005867

Bi, L., Yang, S., Zhao, Y., Wang, Z., Dou, Y., Li, C., et al. (2017). Provenance study of the Holocene sediments in the Changjiang (Yangtze River) estuary and inner shelf of the East China sea. *Quat. Int.* 441, 147–161. doi: 10.1016/j.quaint.2016.12.004

Bianchi, T. S., Cui, X. Q., Blair, N. E., Burdige, D. J., Eglinton, T. I., and Galy, V. (2018). Centers of organic carbon burial and oxidation at the land-ocean interface. *Organ. Geochem.* 115, 138–155. doi: 10.1016/j.orggeochem.2017.09.008

Bianchi, T. S., Mitra, S., and McKee, B. A. (2002). Sources of terrestrially-derived organic carbon in lower Mississippi River and Louisiana shelf sediments: implications for differential sedimentation and transport at the coastal margin. *Mar. Chem.* 77 (2–3), 211–223. doi: 10.1016/S0304-4203(01)00088-3

Blair, N. E., and Aller, R. C. (2012). The fate of terrestrial organic carbon in the marine environment. *Annu. Rev. Mar. Sci.* 4 (1), 401–423. doi: 10.1146/annurev-marine-120709-142717

Boetius, A., Ravenschlag, K., Schubert, C. J., Rickert, D., Widdel, F., Gieseke, A., et al. (2000). A marine microbial consortium apparently mediating anaerobic oxidation of methane. *Nature* 407, 623. doi: 10.1038/35036572

Burdige, D. J. (2007). Preservation of organic matter in marine sediments: controls, mechanisms, and an imbalance in sediment organic carbon budgets? *Chem. Rev.* 107, 467–485. doi: 10.1002/chin.200720266

Cao, C., Cai, F., Zheng, Y., Wu, C., Lu, H., Bao, J., et al. (2018). Temporal and spatial characteristics of sediment sources on the southern Yangtze Shoal over the Holocene. *Sci. Rep.* 8 (1), 15577. doi: 10.1038/s41598-018-33757-5

Chang, X., Liu, X. T., Liu, J. R., Zhang, M. Y., Gu, Y., Wang, N., et al. (2023). Late Quaternary marine transgressions inferred from the pyrite sulfur content and isotopes within core sediments from the southeast coast of China. *Palaeogeogr. Palaeoclimatol. Palaeoecol.* 618, 111513. doi: 10.1016/j.palaeo.2023.111513

Chen, J. Y., Liu, C. Z., Zhang, C. L., and Walker, H. J. (1990). Geomorphological development and sedimentation in Qiantang estuary and Hangzhou Bay. *J. Coastal. Res.* 6, 559–572.

Chen, T., Wang, Z. H., Wu, X. X., Gao, X. Q., Li, L., and Zhan, Q. (2015). Magnetic properties of tidal flat sediments on the Yangtze coast,China: Early diagenetic alteration and implications. *Holocene* 25 (5), 832–843. doi: 10.1177/0959683615571425

Chen, Y. F., Deng, B., and Zhang, J. (2020). Shallow gas in the Holocene mud wedge along the inner East China Sea shelf. *Mar. Petrol. Geol.* 114, 104233. doi: 10.1016/j.marpetgeo.2020.104233

Chen, Y., Zhang, W., Nian, X., Sun, Q., Ge, C., Hutchinson, S. M., et al. (2021). Greigite as an indicator for salinity and sedimentation rate change: evidence from the Yangtze River Delta, China. *J. Geophys. Res.: Solid Earth.* 126, e2020JB021085. doi: 10.1029/2020JB021085

Cheng, H., Zhang, H., Spotl, C., Baker, J., Sinha, A., Li, H., et al. (2020). Timing and structure of the Younger Dryas event and its underlying climate dynamics. *Proc. Natl. Acad. Sci. U. S. A.* 117, 23408–23417. doi: 10.1073/pnas.2007869117

Dávila, P. M., Figueroa, D., and Müller, E. (2002). Freshwater input into the coastal ocean and its relation with the salinity distribution off austral Chile (35–55°S). *Cont. Shelf Res.* 22 (3), 521–534. doi: 10.1016/S0278-4343(01)00072-3

DeLaune, R., and White, J. (2012). Will coastal wetlands continue to sequester carbon in response to an increase in global sea level? a case study of the rapidly subsiding Mississippi river deltaic plain. *Climatic Change.* 110 (1-2), 297–314. doi: 10.1007/s10584-011-0089-6

Dong, J., Li, A. C., Liu, X. T., Wan, S. M., Xu, F. J., and Shi, X. F. (2020). Holocene climate modulates mud supply, transport, and sedimentation on the East China Sea shelf. *J. Geophys. Res. Earth.* 125, e2020JF005731. doi: 10.1029/2020JF005731

Fike, D. A., Bradley, A. S., and Rose, C. V. (2015). Rethinking the ancient sulfur cycle. *Annu. Rev. Earth Pl. Sc.* 43, 593–622. doi: 10.1146/annurev-earth-060313-054802

Gao, Q., Li, Z. L., Chen, Y. T., Zeng, Z. J., Piotrowski, A. M., Yang, S. H., et al. (2023). Implications of sedimentary geochemical characteristics for source-sink processes in Hangzhou Bay since Late Pleistocene. *Geochimica* 1-29. doi: 10.19700/j.0379-1726.2023.01.010

Ge, C., Zhang, W. G., Dong, C. Y., Dong, Y., Bai, X. X., Liu, J. Y., et al. (2015). Magnetic mineral diagenesis in the river-dominated inner shelf of the East China Sea, China. *J. Geophys. Res. Sol Ea.* 120, 4720–4733. doi: 10.1002/2015JB011952

Gomes, M. L., and Johnston, D. T. (2017). Oxygen and sulfur isotopes in sulfate in modern euxinic systems with implications for evaluating the extent of euxinia in ancient oceans. *Geochem. Cosmochim. Acta* 205, 331–359. doi: 10.1016/j.gca.2017.02.020

Goñi, M. A., Ruttenberg, K. C., and Eglinton, T. I. (1998). A reassessment of the sources and importance of land-derived organic matter in surface sediments from the Gulf of Mexico. *Geochim. Cosmochim. Acta* 62, 3055–3075. doi: 10.1016/S0016-7037(98)00217-8

Hedges, J. I., and Oades, J. M. (1997). Comparative organic geochemistry of soils and marine sediments. *Org. Geochem.* 27, 319–361. doi: 10.1016/S0146-6380(97)00056-9

Hepp, D. A., Romero, O. E., Mörz, T., Pol-Holz, R. D., and Hebbeln, D. (2019). How a river submerges into the sea: a geological record of changing a fluvial to a marine paleoenvironment during early Holocene Sea level rise. *J. Quat. Sci.* 34, 581–592. doi: 10.1002/jqs.3147

Hori, K., Saito, Y., Zhao, Q., Cheng, X., Wang, P., Sato, Y., et al. (2001). Sedimentary facies and Holocene progradation rates of the Changjiang (Yangtze) delta, China. *Geomorphology* 41 (2–3), 233–248. doi: 10.1016/S0169-555X(01)00119-27

Hu, Z. A., Li, J., Zhang, W. S., Li, Z. S., Hou, L., and Liu, Q. Y. (2007). Comparison of geochemical characteristics and genesis types of natural gas in the Upper and Lower Paleozoic and Mesozoic in the Ordos Basin. *China Sci.: D-series*, 157–166. doi: CNKI:SUN:JDXK.0.2007-S2-018

Hu, L. M., Guo, Z. G., Feng, J. L., Yang, Z. S., and Fang, M. (2009). Distributions and sources of bulk organic matter and aliphatic hydrocarbons in surface sediments of the Bohai Sea. China. *Mar. Chem.* 113 (3–4), 197–211. doi: 10.1016/j.marchem.2009.02.001

Hu, L. M., Lin, T., Shi, X. F., Yang, Z. S., Wang, H. J., Zhang, G., et al. (2011). The role of shelf mud depositional process and large river inputs on the fate of organochlorine pesticides in sediments of the Yellow and East China seas. *Geophys. Res. Lett.* 38 (3), L03602. doi: 10.1029/2010GL045723

Hu, J. F., Peng, P. A., Jia, G. D., Mai, B. X., and Zhang, G. (2006). Distribution and sources of organic carbon, nitrogen and their isotopes in sediments of the subtropical Pearl River estuary and adjacent shelf, Southern China. *Mar. Chem.* 98, 274–285. doi: 10.1016/j.marchem.2005.03.008

Hu, L. M., Shi, X. F., Yu, Z. G., Lin, T., Wang, H. J., Ma, D. Y., et al. (2012). Distribution of sedimentary organic matter in estuarine-inner shelf regions of the East China Sea: Implications for hydrodynamic forces and anthropogenic impact. *Mar. Chem.* 142-144, 29–40. doi: 10.1016/j.marchem.2012.08.004

Hu, B. Q., Yang, Z. S., Qiao, S. Q., Zhao, M. X., Fan, D. J., Wang, H. J., et al. (2014). Holocene shifts in riverine fine-grained sediment supply to the East China Sea Distal Mud in response to climate change. *Holocene* 24, 1253–1268. doi: 10.1177/0959683614540963

Huang, D. Q., Gao, Q., Li, Z. L., Yang, S. H., Hong, C., Piotrowski, A. M., et al. (2022). Characteristics of clay minerals in sediments of Hangzhou Bay since the Late Pleistocene and their paleoenvironmental significance. *J. Zhejiang Univ. (Science Edition).* 49 (5), 584▪597. doi: 10.3785/j.issn.1008-9497.2022.05.010

Ingram, B. L., Conrad, M. E., and Ingle, J. C. (1996). Stable isotope and salinity systematics in estuarine waters and carbonates: San Francisco Bay. *Geochim. Cosmochim. Acta* 60 (3), 455–467. doi: 10.1016/0016-7037(95)00398-3

Jiang, K. X., Lin, C. M., Zhang, X., Zhao, Y. Y., Lang, X. G., Su, M., et al. (2023). Storm-driven variations in depositional environments modify pyrite sulfur isotope records. *Earth Planet. Sci. Lett.* 610, 118118. doi: 10.1016/j.epsl.2023.118118

Jørgensen, B. B., Findlay, A. J., and Pellerin, A. (2019). The biogeochemical sulfur cycle of marine sediments. *Front. Microbiol.* 10. doi: 10.3389/fmicb.2019.00849

Jørgensen, B. B., and Kasten, S. (2006). Sulfur cycling and methane oxidation. *Mar. Geochem. Springer.* 271–309. doi: 10.1007/3-540-32144-6_8

Kitamura, A., Yamamoto, Y., Yamada, K., Kubo, A., Toyofuku, T., and Nakagawa, Y. (2019). Combined analysis of sulfur and carbon contents, and foraminifer as paleoenvironmental indicators in tidal flat sediments on Miura Peninsula, Japan. *Estuar. Coast. Shelf Sci.* 226, 106256. doi: 10.1016/j.ecss.2019.106256

Lamb, A. L., Wilson, G. P., and Leng, M. J. (2006). A review of coastal and palaeoclimate and relative sealevel reconstructions using $\delta^{13}C$ and C/N ratios in organic material. *Earth Sci. Rev.* 75, 29–57. doi: 10.1016/j.earscirev.2005.10.003

Lambeck, K., Rouby, H., Purcell, A., Sun, Y., and Sambridge, M. (2014). Sea level and global ice volumes from the Last Glacial Maximum to the Holocene. *Proc. Natl. Acad. Sci.* 111, 15296–15303. doi: 10.1073/pnas.1411762111

Leavitt, W. D., Halevy, I., Bradley, A. S., and Johnston, D. T. (2013). Influence of sulfate reduction rates on the Phanerozoic sulfur isotope record. *Proc. Natl. Acad. Sci. U.S.A.* 110, 11244–11249. doi: 10.1091/pnas.1218874110

Li, X., Bianchi, T. S., Allison, M. A., Chapman, P., Mitra, S., Zhang, Z., et al. (2012). Composition, abundance and age of total organic carbon in surface sediments from the inner shelf of the East China Sea. *Mar. Chem.* 145–147, 37–52. doi: 10.1016/j.marchem.2012.10.001

Li, X., Bianchi, T. S., Allison, M. A., Chapman, P., and Yang, G. (2013). Historical reconstruction of organic carbon decay and preservation in sediments on the East China Sea shelf. *J. Geophys. Res.: Biogeosci.* 118, 1079–1093. doi: 10.1002/jgrg.20079

Li, G., Li, P., Liu, Y., Qiao, L. L., Ma, Y. Y., Xu, J. S., et al. (2014). Sedimentary system response to the global sea level change in the East China Seas since the last glacial maximum. *Earth Sci. Rev.* 139, 390–405. doi: 10.1016/j.earscirev.2014.09.007

Li, J. B., Ding, W. W., Wu, Z. Y., and Sun, S. C. (2017). Origin of the east China sea. *Scientia Sin. Terrae.* 47, 406–411. doi: 10.1360/N072017-00006

Li, C. X., Fan, D. D., Yang, S. Y., and Cai, J. G. (2008). Characteristics and formation of the late Quaternary incised valley sequences in estuary and delta areas in China. *J. Palaeogeogr.* 10 (1), 87–97. doi: 10.2110/pec.06.85.0141

Li, G. X., Liu, Y., Yang, Z. G., Yue, S. H., Yang, W. D., and Han, X. S. (2004). Ancient Changjiang channel system in the East China Sea continental shelf during the last glaciation. *Sci. China Seris D: Earth Sci.* 35 (3), 284–289. doi: 10.1360/04yd0053

Lian, E. G., Yang, S. Y., Wu, H., Yang, C. F., Li, C., and Liu, J. T. (2016). Kuroshio subsurface water feeds the wintertime Taiwan Warm Current on the inner East China Sea shelf. *J. Geophys. Res. Oceans.* 121, 4790–4803. doi: 10.1002/2016JC011869

Lin, C. M. (1997). A preliminary sequence stratigraphic study on the Hangzhou Bay, since 15,000 a. B. P. *Geological Rev.* 43 (3), 273~280. doi: 10.16509/j.georeview.1997.03.008

Lin, C. M., Gu, L. X., Li, G. Y., Zhao, Y. Y., and Jiang, W. S. (2004). Geology and formation mechanism of late Quaternary shallow biogenic gas reservoirs in the Hangzhou Bay area, eastern China. *AAPG Bull.* 88 (5), 613–625. doi: 10.1306/01070403038

Lin, C. M., and Zhang, X. (2018). Late quaternary stratigraphy, sedimentology and natural gas geology in the Jiangsu-Zhejiang coastal plain. *Sci. Press Beijing.* 238.

Lin, C. M., Zhang, X., and Huang, S. Y. (2022). Review of Late Quaternary incised valley system. *GEOL. REVIEW.* 68 (2), 627–647. doi: 10.16509/j.georeview.2022.01.031

Lin, C. M., Zhang, X., Xu, Z. Y., Deng, C. W., Yin, Y., and Cheng, Q. Q. (2015). Sedimentary characteristics and accumulation conditions of shallow-biogenic gas for the late quaternary sediments in the changjiang river delta area. *Adv. Earth Sci.* 30 (05), 589–601. doi: 10.11867/j.issn.1001-8166.2015.05.0589

Liu, Y., Deng, L. J., He, J., Zhao, X. S., Wang, H. M., Feng, D., et al. (2021). Holocene geomorphological evolution and the Neolithic occupation in south Hangzhou Bay, China. *Geomorphology* 389, 107827. doi: 10.1016/j.geomorph.2021.107827

Liu, X., Gu, Y., Dong, J., Li, A., Zhuang, G., and Wang, H. (2023). Iron-bearing minerals indicate sea-level rise of the East China Sea inner shelf since the last deglaciation. *Sci. Bull.* 68, 364–366. doi: 10.1016/j.scib.2023.02.002

Liu, M., Hou, L. J., Xu, S. Y., Ou, D. N., Yang, Y., Yu, J., et al. (2006). Organic carbon and nitrogen stable isotopes in the intertidal sediments from the Yangtze Estuary, China. *Mar. pollut. Bull.* 52, 1625–1633. doi: 10.1016/j.marpolbul.2006.06.008

Liu, Q., Kandasamy, S., Lin, B., Wang, H., and Chen, C.-T.-A. (2018). Biogeochemical characteristics of suspended particulate matter in deep chlorophyll maximum layers in the southern East China Sea. *Biogeosciences* 15 (7), 2091–2109. doi: 10.5194/bg-15-2091-2018

Liu, X. T., Li, A. C., Dong, J., Lu, J., Huang, J., and Wan, S. M. (2018). Provenance discrimination of sediments in the Zhejiang-Fujian mud belt, East China Sea: Implications for the development of the mud depocenter. *J. Asian Earth Sci.* 151, 1–15. doi: 10.1016/j.jseaes.2017.10.017

Liu, X. T., Li, A. C., Fike, D. A., Dong, J., Xu, F. J., Zhuang, G. C., et al. (2020). Environmental evolution of the East China Sea inner shelf and its constraints on pyrite sulfur contents and isotopes since the last deglaciation. *Mar. Geol.* 429, 106307. doi: 10.1016/j.margeo.2020.106307

Liu, S. F., Mi, B. B., Fang, X. S., Li, X. Y., Pan, H. J., Chen, M. T., et al. (2017). A preliminary study of a sediment core drilled from the mud area on the inner shelf of the East China Sea: Implications for paleoclimatic changes during the fast transgression period (13 ka BP - 8 ka BP). *Quat. Int.* 441, 35–50. doi: 10.1016/j.quaint.2016.09.057

Liu, J. P., Xu, K. H., Li, A. C., Milliman, J. D., Velozzi, D. M., Xiao, S. B., et al. (2007). Flux and fate of Yangtze River sediment delivered to the East China Sea. *Geomorphology* 85, 208–224. doi: 10.1016/j.geomorph.2006.03.023

Liu, X., Zhang, M., Li, A., Dong, J., Zhang, K., Gu, Y., et al. (2022). Sedimentary pyrites and C/S ratios of mud sediments on the East China Sea inner shelf indicate late Pleistocene-Holocene environmental evolution. *Mar. Geol.* 450, 106854. doi: 10.1016/j.margeo.2022.106854

Liu, X. T., Zhang, M. Y., Li, A. C., Fan, D. D., Dong, J., Jiao, C. Q., et al. (2021). Depositional control on carbon and sulfur preservation onshore and offshore the Oujiang Estuary: Implications for the C/S ratio as a salinity indicator. *Continent. Shelf Res.* 227, 104510. doi: 10.1016/j.csr.2021.104510

Liu, R., and Zheng, H. (2017). Variability of organic carbon isotope and C/N in the Hemudu Area, Hangzhou Bay and its environmental implications in the Holocene. *Geochem. Int.* 55 (12), 1154–1163. doi: 10.1134/S001670291714004X

Loh, P. S., Cheng, L. X., Yuan, H. W., Yang, L., Lou, Z. H., Jin, A. M., et al. (2018). Impacts of human activity and extreme weather events on sedimentary organic matter in the Andong salt marsh, Hangzhou bay, China. *Continent. Shelf Res.* 154, 55–64. doi: 10.1016/j.csr.2018.01.005

Mcleod, E., Chmura, G. L., Bouillon, S., Salm, R., Björk, M., Duarte, C. M., et al. (2011). A blueprint for blue carbon: toward an improved understanding of the role of vegetated coastal habitats in sequestering CO_2. *Front. Ecol. Environ.* 9, 552–560. doi: 10.1890/110004

Milliman, J. D., and Farnsworth, K. (2011). *River Discharge to the Coastal Ocean: A Global Synthesis* Vol. 115–164 (Cambridge: Cambridge Univ. Press), 300. doi: 10.1017/CBO9780511781247

Milne, G. A., Gehrels, W. R., Hughes, C. W., and Tamisiea, M. E. (2009). Identifying the causes of sea-level change. *Nat. Geosci.* 2, 471–478. doi: 10.1038/ngeo544

Mix, A. C., Bard, E., and Schneider, R. (2001). Environmental processes of the ice age: land, oceans, glaciers (EPILOG). *Quat. Sci. Rev.* 20, 627–657. doi: 10.1016/S0277-3791(00)00145-1

Morse, J. W., and Berner, R. A. (1995). What determines sedimentary C-S ratios. *Geochem. Cosmochim. Acta* 59, 1073–1077. doi: 10.1016/0016-7037(95)00024-T

Nesbitt, H. W., and Young, G. M. (1982). Early Proterozoic climate and plat motions inferred from major element chemistry of lutites. *Nature* 299, 715–717. doi: 10.1038/299715a0

Obrist-Farner, J., Brenner, M., Stone, J. R., Wojewóodka-Przybył, M., Bauersachs, T., Eckert, A., et al. (2021). New estimates of the magnitude of the sea-level jump during the 8.2 ka event. *Geology* 50, 86–90. doi: 10.1130/g49296.1

Ouyang, X., Kristensen, E., Zimmer, M., Thornber, C., Yang, Z., and Lee, S. Y. (2023). Response of macrophyte litter decomposition in global blue carbon ecosystems to climate change. *Global Change Biol.* 29 (13), 3806-3820. doi: 10.1111/GCB.16693

Perdue, E. M., and Koprivnjak, J. F. (2007). Using the C/N ratio to estimate terrigenous inputs of organic matter to aquatic environments. *Estuar. Coast. Shelf Sci.* 73, 65–72. doi: 10.1016/j.ecss.2006.12.021

Raiswell, R., and Canfield, D. E. (2012). The iron biogeochemical cycle past and present. *Geochem. Perspect.* 1, 1–220. doi: 10.7185/geochempersp.1.1

Rasmussen, S. O., Bigler, M., Blockley, S. P., Blunier, T., Buchardt, S. L., Clausen, H. B., et al. (2014). A stratigraphic framework for abrupt climatic changes during the Last Glacial period based on three synchronized Greenland ice–core records: refining and extending the INTIMATE event stratigraphy. *Quaternary Sci. Rev.* 106, 14–28. doi: 10.1016/j.quascirev.2014.09.007

Roy, D. K., and Roser, B. P. (2013). Climatic control on the composition of Carboniferous–Permian Gondwana sediments, Khalaspir basin, Bangladesh. *Gondwana Res.* 23 (3), 1163–1171. doi: 10.1016/j.gr.2012.07.006

Sato, H., Hayashi, K. i., Ogawa, Y., and Kawamura, K. (2012). Geochemistry of deep sea sediments at cold seep sites in the Nankai Trough: insights into the effect of anaerobic oxidation of methane. *Mar. Geol.* 323–325, 47–55. doi: 10.1016/j.margeo.2012.07.013

Shen, J., Schoepfer, S. D., Feng, Q., Zhou, L., Yu, J., Song, H., et al. (2015). Marine productivity changes during the end-permian crisis and early triassic recovery. *Earth-Sci. Rev.* 149, 136–162. doi: 10.1016/j.earscirev.2014.11.002

Showers, W. J., and Angle, D. G. (1986). Stable isotopic characterization of organic carbon accumulation on the Amazon continental shelf. *Cont. Shelf Res.* 6, 227–244. doi: 10.1016/0278-4343(86)90062-2

Shu, L. S., Wang, B., Cawood, P. A., Santosh, M., and Xu, Z. (2015). Early Paleozoic and early Mesozoic intraplate tectonic and magmatic events in the Cathaysia block, south China. *Tectonics* 34 (8), 1600–1621. doi: 10.1002/2015TC003835

Shu, J., Wang, W., Jiang, L., and Takahara, H. (2010). Early Neolithic vegetation history, fire regime and human activity at Kuahuqiao, Lower Yangtze River, East China: new and improved insight. *Quat. Int.* 227, 10–21. doi: 10.1016/j.quaint.2010.04.010

Song, L., Fan, D., Su, J., and Guo, X. (2023). Controls on shallow gas distribution, migration, and associated geohazards in the Yangtze subaqueous delta and the Hangzhou Bay. *Front. Mar. Sci.* 10. doi: 10.3389/fmars.2023.1107530

Sun, X. S., Fan, D. J., Hu, L. M., Yang, Z. S., and Guo, Z. G. (2022). Oxidation of petrogenic organic carbon in a large river-dominated estuary. *Geochimica Cosmochimica Acta* 338, 136–153. doi: 10.1016/j.gca.2022.10.028

Sun, X. S., Fan, D., Liao, H., and Tian, Y. (2020). Fate of organic carbon burial in modern sediment within Yangtze River Estuary. *J. Geophys. Res.: Biogeosci.* 124, e2019JG005379. doi: 10.1029/2019JG005379

Tang, M., Yang, S. Y., Li, B. H., Li, C. X., Wang, Q., and Zhao, Q. H. (2006). Compositions of organic carbon and nitrogen and carbon isotope of postglacial sediments in the Yangtze river Delta and the paleoenvironment implication. *Mar. Geol. Quaternary Geol.* 26 (5), 1–10. doi: 10.16562/j.cnki.0256-1492.2006.05.001

Tao, S. Q., Timothy, I. E., Daniel, B., Montluçon, C. M., and Zhao, M. X. (2016). Diverse origins and pre-depositional histories of organic matter in contemporary Chinese marginal sea sediments. *Geochimica Cosmochimica Acta* 191, 70–88. doi: 10.1016/j.gca.2016.07.019

Tesi, T., Miserocchi, S., Goņi, M. A., and Langone, L. (2007). Source, transport and fate of terrestrial organic carbon on the western Mediterranean Sea, Gulf of Lions, France. *Mar. Chem.* 105 (1–2), 101–117. doi: 10.1016/j.marchem.2007.01.005

Wang, Z. H., Bai, Y., He, X. Q., Wu, H., Bai, R. F., Li, T., et al. (2023). Assessing the effect of strong wind events on the transport of particulate organic carbon in the Changjiang River estuary over the last 40 years. *Remote Sens. Environ.* 228C, 113477. doi: 10.1016/j.rse.2023.113477

Wang, Y. J., Cheng, H., Edwards, R. L., An, Z., Wu, J., Shen, C. C., et al. (2001). A high-resolution absolute-dated Late Pleistocene monsoon record from Hulu Cave, China. *Science* 294, 2345–2348. doi: 10.1126/science.1064618

Wang, Y. J., Cheng, H., Edwards, R. L., He, Y. Q., Kong, X. G., An, Z. S., et al. (2005). The holocene Asian monsoon: links to solar changes and North Atlantic climate. *Science* 308, 854–857. doi: 10.1126/science.1106296

Wang, H., Kandasamy, S., Liu, Q., Liu, B., and Chen, C. T. A. (2021). Roles of sediment supply, geochemical composition and monsoon on organic matter burial along the longitudinal mud belt in the East China Sea in modern times. *Geochimica Cosmochimica Acta* 305 (3), 66–86. doi: 10.1016/j.gca.2021.04.025

Wang, W., Li, C., Shu, J., and Chen, W. (2019). Changes of vegetation in southern China. *Sci. China Earth Sci.* 62, 1316–1328. doi: 10.1007/s11430-018-9364-9

Wei, W., and Algeo, T. J. (2020). Elemental proxies for paleosalinity analysis of ancient shales and mudrocks. *Geochem. Cosmochim. Acta* 287, 341–366. doi: 10.1016/j.gca.2019.06.034

Wu, Y., Dittmar, T., Ludwichowskf, K., Kattner, G., Zhang, J., Zhu, Z. Y., et al. (2007). Tracing suspended organic nitrogen from the Yangtze River catchment into the East China Sea. *Mar. Chem.* 107, 367–377. doi: 10.1016/j.marchem.2007.01.022

Xu, R. Y. (1995). Formation and migration of the water system of Qiantang River. *Geol. Zhejiang.* 11, 40–48.

Xu, Y., Yu, C., Zhang, P., Deng, X., Zhang, Z., and Shen, H. (2019). Spring nekton community structure and its relationship with environmental variables in Hangzhou Bay-Zhoushan inshore waters. *J. Fish. China.* 43 (3), 605–617. doi: 10.11964/jfc.20180511303

Yang, X. D., Chun, M. H., Luo, X. Q., and Yao, Z. G. (2022). Research on application of seismic attribute analysis in identification of subsea shallow gas. *Coast. Eng.* 01, 26–36.

Yuan, H. W., Chen, J. F., Ye, Y., Lou, Z. H., Jin, A. M., Chen, X. G., et al. (2017). Sources and distribution of sedimentary organic matter along the Andong salt marsh, Hangzhou Bay. *J. Mar. Sys.* 174, 78–88. doi: 10.1016/j.jmarsys.2017.06.001

Zhang, X., Dalrymple, R. W., Yang, S. Y., Lin, C. M., and Wang, P. (2015). Provenance of Holocene sediments in the outer part of the Paleo-Qiantang River estuary, China. *Mar. Geol.* 366, 1–15. doi: 10.1016/j.margeo.2015.04.008

Zhang, W., Jin, H., Zhang, F., Zhao, G., Yang, K., Li, H., et al. (2009). Organic Carbon distribution in the Yangtze River Estuary-Hangzhou Bay and its adjacent sea area. *Adv. Earth Sci.* 24, 1202–1209. doi: 10.11867/j.issn.1001-8166.2009.11.1202

Zhang, K. D., Li, A. C., Huang, P., Lu, J., Liu, X. T., and Zhang, J. (2019). Sedimentary responses to the cross-shelf transport of terrigenous material on the East China Sea continental shelf. *Sediment. Geol.* 384, 50–59. doi: 10.1016/j.sedgeo.2019.03.006

Zhang, X., Lin, C., Dalrymple, R. W., Gao, S., and Li, Y. (2014). Facies architecture and depositional model of a macrotidal incised-valley succession (Qiantang River estuary, eastern China), and differences from other macrotidal systems. *Geol. Soc. America Bullet.* 126, 499–522. doi: 10.1130/B30835.1

Zhang, X., Lin, C. M., Dalrymple, R. W., and Yang, S. Y. (2021). Source-to-sink analysis for the mud and sand in the late-quaternary Qiantang river incised-valley fill and its implications for delta-shelf-estuary dispersal systems globally. *Sedimentology* 68 (7), 3228–3252. doi: 10.1111/SED.12901

Zhang, J., Meng, X. W., and Wang, X. Q. (2013). The record of major element ratios in Late Quaternary at northern slope of the South China Sea and its indicative significance on the cooling events. *Acta OCEANOL Sin.* 35 (4), 106–111. doi: 10.3969/j.issn.0253-4193.2013.04.013

Zhao, B., Yao, P., Bianchi, T. S., and Yu, Z. G. (2021). Controls on organic carbon burial in the eastern China marginal seas: a regional synthesis. *Global Biogeochem. Cycles* 35, e2020GB006608. doi: 10.1029/2020GB006608

Zhao, G., Ye, S., Laws, E. A., He, L., Yuan, H., Ding, X., et al. (2019). Carbon burial records during the last 40,000 years in sediments of the Liaohe delta wetland, China. *Estuar. Coast. Shelf Sci.* 226 (OCT.15), 106291.1–106291.10. doi: 10.1016/j.ecss.2019.106291

Zheng, Y., Zheng, H. B., Kissel, C., and Laj, C. (2011). Sedimentation rate control on diagenesis, East China Sea sediments. *Phys. Earth Planet. In.* 187, 301–309. doi: 10.1016/j.pepi.2011.05.005

Zhou, J. L., Wu, Y., Zhang, J., Kang, Q. S., and Liu, Z. T. (2006). Carbon and nitrogen composition and stable isotopes as potential indicators of source and fate of organic matter in the salt marsh of the Changjiang Estuary, China. *Chemosphere* 65, 310–317. doi: 10.1016/j.chemosphere.2006.02.026

Zhou, X., Zhan, T., Tu, L. Y., Smol, J. P., Jia, S. W., Liu, X. Y., et al. (2022). Monthly insolation linked to the time-transgressive nature of the Holocene East Asian monsoon precipitation maximum. *Geology* 50, 331–335. doi: 10.1130/G49550.1

Zhu, M.-X., Chen, K.-K., Yang, G.-P., Fan, D.-J., and Li, T. (2016). Sulfur and iron diagenesis in temperate unsteady sediments of the East China Sea inner shelf and a comparison with tropical mobile mud belts (MMBs). *J. Geophys. Res. Biogeo* 121, 2811–2828. doi: 10.1002/2016JG003391

Zong, Y. Q. (2004). Mid-Holocene sea-level highstand along the Southeast Coast of China. *Quaternary Int.* 117, 55–67. doi: 10.1016/S1040-6182(03)00116-2

Zong, Y., Lloyd, J. D., Leng, M. J., Yim, W. W.-S., and Huang, G. Q. (2006). Reconstruction of the Holocene monsoon history from the Pearl River Estuary, southern China, using diatoms and organic carbon isotope ratios. *Holocene* 16, 251–263. doi: 10.1191/0959683606hl911rp